The $\nu 1$, $\nu 4$ and $3\nu 6$ bands of methyl chloride in the 3.4 μm region: line positions and intensities

Cédric Bray, Agnes Perrin, David Jacquemart, Nelly Lacome

The ν_1, ν_4 and $3\nu_6$ bands of methyl chloride in the 3.4 µm region: line positions and intensities

C. Bray [a,b], *A. Perrin* [c], *D. Jacquemart* [a,b], *N. Lacome* [a,b]

[a] UPMC Univ Paris 06, Laboratoire de Dynamique, Interactions et Réactivité, UMR 7075, Case Courrier 49, 4 Place Jussieu, 75252 Paris Cedex 05, France

[b] CNRS, UMR 7075, Laboratoire de Dynamique, Interactions et Réactivité, Case Courrier 49, 4 Place Jussieu, 75252 Paris Cedex 05, France

[c] Laboratoire Interuniversitaire des Systèmes Atmosphériques, LISA-UMR7583, CNRS and Universités Paris Est Créteil (UPEC) and Paris Diderot- Paris 7, 61 avenue du Général de Gaulle, 94010 Créteil cedex, France

The authors would like to dedicate this paper to the memory of Dr. Curt P. Rinsland.

Number of Figures: 9

Number of Tables: 12

Number of Appendix: 1

Please send proofs to: Agnès Perrin

Email: Agnes.perrin@lisa.u-pec.fr

Tel. 33(0)14517 6557, Fax. 33(0)145171564

Abstract

Methyl chloride (CH_3Cl) is one of the most abundant chlorine-containing molecules in the atmosphere. For this reason a recent update was performed by Iouli Gordon (private communication) in HITRAN in the 640-2600 cm^{-1} region using line parameters generated by A. Nikitin, et al. [Nikitin A Champion JP, and Bürger H. J Mol Spectrosc 2005;230:174-184]. CH_3Cl has a rather strong signature around 3000 cm^{-1} which was used recently by the Atmospheric Chemistry Experiment (ACE) satellite mission to produce the first study of the global distribution of methyl chloride in the upper troposphere and stratosphere. However it was mentioned that the CH_3Cl line positions and intensities spectroscopic parameters are of very low quality in this spectral region in the public access HITRAN or GEISA databases. We present a complete update of the line positions and line intensities for the ν_1, ν_4, $3\nu_6$ bands of $CH_3{}^{35}Cl$ and $CH_3{}^{37}Cl$ in the 3.4 µm region. For this task, Fourier transform spectra have been recorded at high resolution in "Laboratoire de Dynamique, Interactions et Réactivité" (LADIR). Measurements of line positions and line intensities have been retrieved for both isotopologues $^{12}CH_3{}^{35}Cl$ and $^{12}CH_3{}^{37}Cl$ in the ν_1, ν_4, $3\nu_6$ bands. The theoretical model accounts for the interactions coupling the (v_1=1; ℓ =0), (v_4=1; ℓ =±1) and (v_6=3; ℓ =±1) energy levels, together with additional resonances involving several dark states.

1. Introduction

One of the most abundant chlorine-containing molecules in the atmosphere is methyl chloride (CH_3Cl); a species whose sources are almost entirely natural. The most common sources of methyl chloride are tropical plants, withering or dead leaves and biomass burning. As the impacts of the Montreal Protocol and its subsequent amendments are becoming apparent in the reduction of chlorofluorocarbons in the atmosphere, naturally- produced methyl chloride is playing an increasingly significant role in the atmospheric ozone budget. Solar occultation measurements performed from the infrared Fourier transform spectrometer (ACE-FTS) on board the Atmospheric Chemistry Experiment (ACE) satellite mission have been used recently to produce the first study of the global distribution of methyl chloride in the upper troposphere and stratosphere [1]. For this task, the retrievals of CH_3Cl abundances from atmospheric infrared spectra rely on the observation of the *Q*-branch structures of the ν_1^0 band of CH_3Cl in the 3.4 µm region. The atmospheric retrievals require accurate spectroscopic parameters especially for line positions and intensities.

For the 3.4 µm region the HITRAN [2] or GEISA [3] linelist for CH_3Cl covers the 2907.8-3182.9 cm^{-1} region. Figure 1 gives an overview of the 3.4 µm infrared absorption region which corresponds to the strong ν_1^0 band and to the two times weaker ν_4^1 and $3\nu_6^1$ and $2\nu_5^0$ bands. The band notation ν_4^1 (for example) with $|\ell|$ as superscript corresponds to the vibrational transition between the (ν_4=1; ℓ =±1) state and the ground state. Also ℓ refers to $\sum_i \ell_i$, where the ℓ_i are the vibrational angular momentum quantum numbers associated to degenerated modes. As evidenced in Fig. (2) the most striking deficiencies of the linelist available in the public access databases concern the strong ν_1^0 band for which the list is restricted to several ${}^QQ_K$ structures (for *K*= 1 to 6) in the 2965.7 to 2968.6cm^{-1} region. Although this list contains numerous lines from the weak ν_4^1 and $3\nu_6^1$ bands, the much stronger *P*- and *R*-lines of the ν_1^0 band are completely missing, and this is evidenced on Fig. (3) which details a portion of the *P*-branch of the ν_1^0 band.

This is a problem for the atmospheric retrievals performed at 3.4 µm, not only for CH_3Cl, but also for several atmospheric target species, for example ethane (C_2H_6), for which CH_3Cl acts as an interfering molecule at 3.4 µm.

The $CH_3{}^{35}Cl$ and $CH_3{}^{37}Cl$ list present at 3.4 µm in HITRAN [2] or GEISA [3] takes its origin from rather old spectroscopic studies. Only the most recent ones will be mentioned here.

The line positions of the $\nu_1{}^0$ band were investigated by Morillon et al. [4] using grating spectra recorded at medium resolution (0.030 cm^{-1}) and then latter by Dang-Nhu [5] by Fourier transform spectroscopy, and no noticeable perturbations was noticed during the $\nu_1{}^0$ band investigation. In Ref. [6], the analysis of the $\nu_4{}^1$, and $3\nu_6{}^1$ interfering bands was performed by combining Fourier transform spectra recorded at 0.0074 cm^{-1} resolution with Raman data. Only the strong resonances coupling the ($v_4=1; \ell = \pm 1$) and ($v_6=3; \ell = \pm 1$) energy levels were accounted for during the energy levels calculations. The results were satisfactory, in general, although several perturbed series (starting from K=7) had to be excluded from the calculation. It is presumed [7] that the ($v_2=1, v_3=1, v_6=1; \ell = \pm 1$) and/or ($v_6=3; \ell = \pm 3$) and/or ($v_1=1; \ell = 0$) energy levels are involved in the observed perturbations.

The available data for intensities are rather sparse. Low and medium intensities measurements have been reported in the past [8, 9]. The first individual line intensities measurements at 3.4 µm were performed using a single high resolution FTS spectrum by Dang-Nhu and co workers in Refs. [5] and [10], for the $\nu_1{}^0$ band and for the $\nu_4{}^1$ and $3\nu_6{}^1$ interfering bands, respectively. Because of its consistency with the results issued from these studies, it is highly presumed that the HITRAN [2] or GEISA [3] line list for CH_3Cl at 3.4 µm originates from Dang-Nhu et al studies [5, 10]. More recently, cross sections were measured for CH_3Cl at 0.06 cm^{-1} resolution in the whole 600-6600 cm^{-1} spectral range at Pacific Northwest National Laboratory [11].

The present work is a thorough analysis of the ν_1^0, ν_4^1, and $3\nu_6^1$ bands of methyl chloride, relying on high-resolution Fourier transform absorption spectra recorded at the LADIR. Absolute line positions and intensities have been measured for 182 transitions of $^{12}CH_3{}^{35}Cl$ and 378 transitions of $^{12}CH_3{}^{37}Cl$ of these three bands using a multispectrum fitting procedure. Moreover 3451 and 1371 positions of $^{12}CH_3{}^{35}Cl$ and $^{12}CH_3{}^{37}Cl$ transitions respectively have been obtained from a peak finding procedure and assigned. An accurate set of vibrational energies, and rotational, anharmonic and Coriolis constants was obtained for the (v_1=1; ℓ =0), (v_4=1; ℓ =±1) and (v_6=3; ℓ =±1) interacting vibrational states. For this calculation it was necessary to account for additional resonances involving the (v_3=2,v_5=1; ℓ =±1), (v_5=2; ℓ =±2) and (v_6=3; ℓ =±3) dark resonating states. Additionally, absolute line intensities have been calculated, and a list of line positions and intensities was generated, including information for the ν_1^0, ν_4^1, $3\nu_6^1$ bands for both $^{12}CH_3{}^{35}Cl$ and $^{12}CH_3{}^{37}Cl$ isotopic species. Finally, it should be mentioned that the present analysis does not involve the weaker $2\nu_5^0$ band centered near 2880 cm^{-1}, which is extremely perturbed [12-14] and of less interest for atmospheric applications.

2. Experimental conditions

Six Fourier transform spectra have been recorded using the rapid scan Bruker IFS 120 HR interferometer of the LADIR. The experimental conditions are summarized in Table 1. The interferometer was equipped with CaF_2 beam splitter, InSb detector, globar source, and an optical filter covering the 2800-3200 cm^{-1} spectral region. For spectrum #3, no optical filter has been used for recording the whole 1800-5000 cm^{-1} spectral range. This allowed observing CO_2 and H_2O impurities present in the interferometer. The transitions of CO_2 near 2300 cm^{-1} and of H_2O near 1900 and 3700 cm^{-1} have been used to perform the wavenumber calibration (see Section 3.2). The whole optical path was under vacuum, and a single pass (30.00 ± 0.05) cm cell equipped with KCl windows was used. The commercial gas sample, furnished by Alpha Gaz, with a stated of purity of 99.9% in natural abundances, was used without any purification. All spectra have been recorded at room temperature. Spectra #3 and #4 are plotted in Fig. 4, showing the good quality of experiments. The pressure of the gas was measured with 2 baratron gauges with an accuracy better than ± 0.15% for that of 1 mbar full scale and ± 0.25% for that of 10 mbar full scale. The average interferogram has been Fourier

transformed using the procedure included in the Bruker software OPUS package, selecting a Mertz phase error correction. The spectra have not been numerically apodized.

3. Measurements

To measure as many as possible transitions, a multispectrum fitting procedure [15] was used to retrieved line parameters. Since methyl chloride has a large dipole moment, the effect of the self broadening on the line profile is significant [16] (self-broadening width at 5 mbar is nearly equal to the Doppler width at 3000 cm^{-1}). The line intensity measurement is strongly dependent on the broadening coefficient, so that accurate measurements of line intensities need an adjustment of the self-broadening coefficients. The self-broadening coefficients will be presented in a forthcoming paper dealing also with N_2 widths. For all spectra, a Voigt profile was used and no deviation from this profile was observed in the residuals. An example of a fit is given in Fig. 5.

The measurements of line positions and intensities have been used to adjust the constants of the theoretical model described in sections 5-7 respectively.

3.1. Apparatus function and baseline

For each spectrum, the apparatus function was calculated performing numerically the Fourier transform of the optical weighting function of the interferogram, taking into account the effect of the throughput and of the finite optical path difference [17]. In the definition of the apparatus function, the aperture and the focal length of the collimator are sensitive parameters. The nominal value of the focal length (418 mm) was used as well as an effective value of the aperture found close (0.80 mm) to the nominal value (0.75 mm). To determine this effective value, the iris radius was fitted on isolated lines in spectrum #3 for which CH_3Cl, H_2O and CO_2 transitions are simultaneously observed. The average value of the aperture was found equal to (0.80±0.04) mm for the 90 fitted transitions and no wavenumber dependence was observed. The effect on the line parameter retrievals is not negligible even if this average value is close to the nominal one. It can amount to a few percent (1-3% depending on the deepness of the transitions) on line intensity and broadening coefficients.

Also a multiplicative channel spectrum, due to the cell windows, was observed in all experimental spectra. Its period is around 0.60 cm^{-1} with maximum peak to peak amplitude of

about 5 %. Because the adjusted spectral domains used are always less than the half-period of the channel, it can be reproduced by the polynomial expansion that adjusts the continuous background.

3.2. Wavenumber calibration

The HITRAN [2] wavenumbers of CO_2 transitions around 2300 cm^{-1}, and for H_2O transitions around 1900 and 3600cm^{-1} [2] were taken as etalons. The quantity $\varepsilon = (\nu_{HITRAN2008} - \nu_{this\ work}) / \nu_{HITRAN2008}$ was calculated from spectrum #3, and an average value was deduced: $<\varepsilon> = 1.8\times10^{-7}$, which corresponds to a wavenumber deviation of 0.6×10^{-3} cm^{-1} at 3000 cm^{-1} with a scattering (1SD) of 0.1×10^{-3} cm^{-1}. Considering the scattering of the wavenumber calibration, and the accuracy of the CO_2 and H_2O line positions, the accuracy of measured wavenumbers was estimated to be better than 0.5×10^{-3} cm^{-1}.

4. Rovibrational analysis

Figure 1 presents an overview of the $2\nu_5^0$, ν_1^0, ν_4^1 and $3\nu_6^1$ bands of methyl chloride in the 2850-3300 cm^{-1} region. The analysis proved to be rather easy for the ν_1^0 band, but difficult for the ν_4^1, $3\nu_6^1$ bands which are weaker and exhibit strong perturbations. As it will be discussed later, at least three additional dark states are responsible for the perturbations observed on the (v_1=1; ℓ =0), (v_4=1; ℓ =±1) and (v_6=3; ℓ =±1) energy levels. According to symmetry considerations, for a C_{3v}-type molecule, ν_1^0 is a parallel band, while ν_4^1 and $3\nu_6^1$ are perpendicular bands. Finally let us remember the extreme complexity of the $2\nu_5^0$ band [12-14]: this weak band which has low atmospheric interest was not considered in the present study.

The first ν_1^0, ν_4^1 and $3\nu_6^1$ assignments were performed using calculated predictions both for line positions and relative line intensities. The ground state energy levels were computed using a standard symmetric-top Hamiltonian (see appendix Eq.(A1)) together with the rotational and centrifugal distortion constants quoted in Ref. [18]. For the upper states the preliminary set of vibrational energies, rotational and interacting constants from Refs. [4] and [6] were used for the calculation of the (v_1=1; ℓ =0) and of (v_4=1; ℓ =±1) and (v_6=3; ℓ =±1) energy levels, respectively. As in Ref. [6] the (v_4=1; ℓ =±1) and (v_6=3; ℓ =±1) upper state

energy levels were computed accounting for the anharmonic and Z-type Coriolis interactions which couple these energy levels. For the preliminary list of predictions, the relative intensities of the ν_1^0, ν_4^1 and $3\nu_6^1$ bands were computed using the theoretical method described in paragraph 5 and using the intensity parameters delivered by [5, 10] for the ν_1^0 and ν_4^1 fundamental bands. Indeed, as an overtone, the $3\nu_6^1$ band is in principle a dark band but is observable because strong anharmonic and Coriolis resonances couple the (v_4=1; ℓ =±1) and (v_6=3; ℓ =±1) interacting energy levels [6]. Some low and medium *J* and *K* transitions for the ν_1^0, ν_4^1 and $3\nu_6^1$ bands were first assigned for both isotopic species. Then, using the ground state parameters of Ref. [18], the lower state energy levels were calculated and added to the newly observed line positions to get a list of experimental upper state energy levels. These upper state levels were included in a least squares fit to get an improved set of upper states parameters allowing better predictions and hence more assignments to be made. At a given level, it was necessary to account for ($\Delta\ell$ =±1;ΔK=±1,) resonances coupling the (v_1=1; ℓ =0) energy levels with those from the (v_4=1; ℓ =±1) and (v_6=3; ℓ =±1) vibrational states. In addition resonances coupling the (v_1=1; ℓ =0), (v_4=1; ℓ =±1) and (v_6=3; ℓ =±1) with those from the (v_3=2,v_5=1; ℓ =±1), (v_5=2; ℓ =±2) and (v_6=3; ℓ =±3) dark states had to be considered during the assignments.

This iterative process was carried out until the complete assignment of the ν_1^0 and the ν_4^1 and $3\nu_6^1$ bands for both isotopic species.

The results of the final assignments are given in the upper part of Table 2. Because of the existence of numerous resonances involving the (v_3=2,v_5=1; ℓ =±1), (v_5=2; ℓ =±2) and (v_6=3; ℓ =±3) dark states, it was possible to identify several transitions belonging to the $2\nu_3+\nu_5^1$ and $3\nu_6^3$ associated dark bands. Examples of such assignments are given in Figs. 2-3 and 6-8. Table 2 shows that the range of upper state rotational energy levels covered by the present analysis is significantly extended as compared to the previous ones [4-6]. Indeed, the previous investigations were restricted to $|K|\leq 6$ for the ν_1^0 band [4, 5], and up to $|K|\leq 7$ and $J\leq 28$ for the ν_4^1 and $3\nu_6^1$ bands [6].

5. Energy levels calculation

The list of CH_3Cl normal modes and vibrational energies is given in Table 3. A global fit of the lower five polyads of interacting states (fundamental and overtones or combination states) in the 0 to 2600 cm^{-1} was performed by Nikitin et al [19]. The vibrational energies for vibrational states existing in the 0-3480 cm^{-1} energy range were calculated for $CH_3{}^{35}Cl$ and $CH_3{}^{37}Cl$ from a full dimensional ab initio surface [7]. According to Table 5 in Ref. [7], numerous dark states exist in the 2700-3200 cm^{-1} energy range which are potentially responsible for resonances perturbing the energy levels of the bright (v_1=1; ℓ =0) and (v_4=1; ℓ =±1) states and of the (v_6=3; ℓ =±1) dark state.

The types of anharmonic or Coriolis resonances which can be observed during the analysis of the spectra are numerous. This is expected when examining the resonances which had to be considered for the polyads P3 to P5 [16, 19-24].

The situation for vibrational states located above 2500 cm^{-1} (polyad P6) is even more complex [12-14]. By extrapolating from the resonance scheme in polyads P3 to P5 (see Tables 3 and 4 in Ref. [19]) it is presumed that, gradually, all overtones or combination states from the (v_2=2; ℓ =0) up to the (v_3=v_5=v_6=1; ℓ = 0 and ℓ =2) (A_1, A_2 and E symmetry near 3184-3190 cm^{-1}) are more or less coupled through various resonances. From extended studies performed in the 2650-2950 cm^{-1} region [13, 14] only positions of some dark bands, namely $\nu_3+2\nu_6{}^0$, $\nu_2+2\nu_3{}^0$, $\nu_2+\nu_5{}^1$, $2\nu_5{}^0$, $2\nu_5{}^2$, and $2\nu_3+\nu_5{}^1$, could be obtained for $^{12}CH_3{}^{35}Cl$ and $^{12}CH_3{}^{37}Cl$, with an accuracy of ~0.1 cm^{-1}.

For this reason, the strategy that was adopted here was empirical. In a first step, our energy levels calculation was restricted to the system of (v_1=1; ℓ =0), (v_6=3; ℓ =±1) and (v_4=1; ℓ =±1) interacting states. However, several additional local resonances were observed during the assignment process, and three dark states, (v_3=2,v_5=1; ℓ =±1), (v_5=2; ℓ =±2), and (v_6=3; ℓ =±3) were identified as responsible for most of the observed perturbations. So, the final calculation involved, altogether the {(v_5=2; ℓ =±2), (v_3=2,v_5=1; ℓ =±1), (v_1=1; ℓ =0), (v_6=3; ℓ =±1), (v_6=3; ℓ =±3), (v_4=1; ℓ =±1)}, interacting states, neglecting the perturbations due to other dark states. Therefore, as a general conclusion, it is clear that the model used in this work for the energy level calculation is effective.

The general form of the Hamiltonian matrix used to compute the energy levels is given in Table 4. As discussed in Refs. [25-27], it is important to define precisely the phase factor of the wavefunctions. In the present work the convention of Refs. [28-30] was adopted and

differs from the one adopted by Fusina and Di Lonardo [31], and Pracna et al. [25, 32-34]. The diagonal and off diagonal matrix elements are given in Appendix (Eqs. (A1 to A10)). As usual, both essential and accidental resonances were considered.

The experimental {(v_5=2; ℓ =±2), (v_3=2,v_5=1; ℓ =±1), (v_1=1; ℓ =0), (v_4=1; ℓ =±1), (v_6=3; ℓ =±1), (v_6=3; ℓ =±3)} energy levels obtained in this work were introduced in a least squares fit procedure using this Hamiltonian model. For $CH_3{}^{37}Cl$, all the observed energy levels were considered in this calculation. As compared to the ^{37}Cl variant, the analysis for $CH_3{}^{35}Cl$ could be performed up to higher *J* and *K* values, but some perturbed series belonging to the (v_4=1; ℓ =±1), and involving high *K* values (|*K*| ≥8) had to be excluded from the fit. One of the possible explanations is in the existence of resonances involving dark states located at energies above 3060 cm^{-1}. For example states as (v_2=1,v_3=1,v_6=1; ℓ =±1), or (v_3=3,v_6=1; ℓ =±1) located near 3088 and 3173 cm^{-1} respectively [7], are not considered in the present model. Let us remember that except for the 4250-4600 cm^{-1} spectral region [35] no high-resolution investigation exists for methyl chloride infrared bands located at wavenumbers higher than 3050 cm^{-1}.

Tables 5 and 6 list the Hamiltonian constants resulting from the fit for $CH_3{}^{35}Cl$ and $CH_3{}^{37}Cl$, respectively, together with their associated statistical uncertainties. In these tables, the constants without uncertainties were fixed to their ground state values [18]. Because of the suspected existence of additional interactions, the parameters gathered in Tables 5 and 6 are effective, with poor physical meaning. The results of the energy levels calculations proved to be rather satisfactory, as can be seen from the standard deviation and statistical analyses given in the lower part of Table 2.

6. Discussion

It is useful to describe the wavefunctions resulting from the diagonalization of the upper and lower state Hamiltonian matrices. In the upper state, the considered |Γ, v′ ℓ ′, *J K*> wavefunctions are written as:

$$\left|\Gamma = A\ , \mathrm{v}'\ \ell', J'K'\ \right\rangle = \sum_{\mathrm{v}\ell \in B'} \ \sum_{K,\gamma}\ {}^{A}C_{\mathrm{v}\ell}^{\gamma\ K}\ \left|\ \mathrm{v}\ell\right\rangle \left|\ell, JK\,\gamma\ \right\rangle, \qquad (1,a)$$

with A= A_1 or A_2.

$$\left|\Gamma = E, \mathrm{v}'\,\ell', J'K' \right\rangle = \sum_{\mathrm{v}\ell \in B'} \sum_{K} {}^{E}C_{\mathrm{v}\ell}^{K} \left| \mathrm{v}\ell \right\rangle \left| \ell, JK \right\rangle \qquad (1,b)$$

In Eqs. (1), the ${}^{\Gamma}C_{\mathrm{v}\ell}^{\gamma K}$ coefficients result from the diagonalization of the upper state Hamiltonian matrix and B' = {(v_5=2; ℓ =±2), (v_3=2,v_5=1; ℓ =±1), (v_1=1; ℓ =0), (v_4=1; ℓ =±1), (v_6=3; ℓ =±1), (v_6=3; ℓ =±3)} is the set of interacting states. The expansions in Eqs. (1) are performed on a set of wavefunction basis set which depend on the symmetry (Γ=A_1, A_2 or E) of the considered |Γ, v′ ℓ ′, *J K*> energy level.

For Γ=A_1 and A_2 symmetries (*K*- ℓ = ±3n), the | ℓ , *J K* γ> in Eqs. (1.a), are the Wang-type wavefunctions defined as:

$$\left|\ell, J\,K\,\gamma\right\rangle = {}^{1}\!/_{\sqrt{2}} \left|\ell, JK\right\rangle + \gamma\left|-\ell, J-K\right\rangle \text{ , for } K\text{-}\ell = \pm 3n \text{ and } (\ell \neq 0 \text{ or } K \neq 0), \qquad (2)$$

with $\gamma = -1^{\,J+K+\ell}$ and $\gamma = -1^{\,J+K+\ell+1}$ for A_1 and A_2 symmetry, respectively.
Finally, one has:

$$\left|\ell = 0, J\,K = 0\ \gamma = +1\right\rangle = \left|\ell = 0, J\,K = 0\right\rangle \text{ for } \ell = 0 \text{ and } K = 0. \qquad (3)$$

For E symmetry (see Eq. (1,b)), the base functions are the usual non–symmetrized wave basis functions defined as:

| ℓ , *J K*>. with *K*- ℓ =1±3n (4)

Indeed, because of the E-type degeneracy, the wavefunctions in *K*- ℓ =2±3n and *K*- ℓ =1±3n lead to equal eigenvalues.

In the present case we are dealing only with cold bands, and the lower state is the ground state with ℓ =0. In this case, the set of lower state wavefunctions |Γ, v"=0 ℓ "=0, *J*" *K*"> coincide with the set of basis wavefunctions defined in Eqs. (2-4).

As already discussed, we observed strong resonances between the energy levels of vibrational sates belonging to the polyad B' = {(v_5=2; ℓ =±2), (v_3=2,v_5=1; ℓ =±1),

(v_1=1; ℓ =0), (v_6=3; ℓ =±1), (v_6=3; ℓ =±3), (v_4=1; ℓ =±1)}. To stress this point, it is useful to define the mixing coefficient (in percentage) noted %(Γ,' v′ ℓ ′, *J*′ *K*′| v ℓ) of a given |Γ', v′ ℓ ′, *J*′ *K*′> energy level on another vℓ ≠ v′ℓ ′ interacting vibrational states of the B' polyad :

$$\%\ \Gamma', v'\ell', J'K'|v\ell\ = \sum_k \left|{}^{\Gamma}C_{v\ell}^{\gamma K}\right|^2 \times 100 \qquad (5)$$

Table 7 summarizes the main resonances observed during the present study. One has to stress that the resonance scheme is consistent for both $CH_3{}^{35}Cl$ and $CH_3{}^{37}Cl$.

As an example, Fig. 9 gives the mixing percentages for the (v_4=1; ℓ =±1) energy levels of $CH_3{}^{35}Cl$ with *J*=21 and A_1 symmetry. As it is the case for all *J* values, strong mixings couple together the (v_4=1; ℓ =±1) ⇔ (v_6=3; ℓ =±1) energy levels. In addition, for *J*=21, there exists a local resonance coupling together (v_4=1; ℓ =±1), *K*=-2 ⇔ (v_6=3; ℓ =±1) *K*=0. Accordingly the $v_4{}^1{}^P Q_{K''=-3}$ branch (see Fig. 7) is strongly perturbed.

7. Line intensity calculation:

The absolute line intensity $k_{\tilde{\nu}}^N$ (integrated over one line, given in cm^{-1}/(molecule.cm^{-2}) for CH_3Cl in natural abundance) of a transition between a lower level *L* of energy E_L and an upper level *U* of energy E_U can be expressed as:

$$k_{\tilde{\nu}}^N = I_a \frac{8\pi^3\tilde{\nu}}{4\pi\varepsilon_0 3hc\ \ Q(T)} g_{nucl}^{Cl} . g_{nucl}^{H} \left(1-\exp\left(-\frac{hc\tilde{\nu}}{kT}\right) \right) \exp\left(-\frac{hcE_L}{kT}\right) R_L^U \qquad (6)$$

where *T* is the temperature in Kelvin, $\tilde{\nu}$ =(E_U–E_L)/hc is the line position (in cm^{-1}), I_a = 0.748937 and 0.239491 is the isotopic abundance of $^{12}CH_3{}^{35}Cl$ and $^{12}CH_3{}^{37}Cl$, respectively [36]. In this expression g_{nucl}^{Cl} and g_{nucl}^{H} are the nuclear statistical weights due to the chlorine and hydrogen nuclear spins of the lower level (I=3/2 and I=1/2 for Cl and H, respectively),

with g_{nucl}^{Cl} = 4 for all levels, and g_{nucl}^{H} = 4:4:4 for the A_1:A_2:E symmetries, respectively. Also $Q(T)$ is the total internal partition function for which we used values consistent with those quoted in HITRAN [2] (Q(296K) = 57916.1 and 58833.9 at 296 K [37] for $^{12}CH_3{}^{35}Cl$ and $^{12}CH_3{}^{37}Cl$, respectively).

Q_{vib}(296K)=1.0475
(7)

R_L^U is the square of the matrix element of the transformed dipole moment operator $\mu_Z^{'}$:

$$R_L^U = \left|\left\langle \mathrm{v}'\ell', J'K' \left| \mu_Z^{'} \right| \mathrm{v}''\ell'', J''K'' \right\rangle\right|^2 \quad (8)$$

where (v";ℓ") and (v′;ℓ′) and J" K" and J' K' are the vibrational and rotational quantum numbers, respectively, in the lower and upper levels of the transition. Since we are dealing only with cold bands, and because the CH_3Cl ground state is non degenerate (ℓ"=0), the values (v"=0;ℓ"=0) are set as |0> in the following. The expansion of the upper state rovibrational wavefunctions is given in Eqs (1) according to the symmetry (A_1, A_2 or E) of the considered energy level. The transformed dipole moment operator $\mu_Z^{'}$ can be expanded as:

$$\mu_Z^{'} = \sum_{\mathrm{v}'\in B'} |0\rangle \, {}^{\mathrm{v}'}\mu_Z^{\Delta\ell} \, \langle \mathrm{v}'\ell' | \quad (9)$$

where ${}^{\mathrm{v}'}\mu_Z^{\Delta\ell}$ is the transformed dipole moment operator corresponding to the transition |0> → |v'; ℓ' >.

By extension from the asymmetric-top molecules model [38] and using the phase convention of Refs. [28-30, 39], the expansion of the transformed transition dipole moment operator for a given $\Delta\ell = 0$ parallel band (for example the $\nu_1{}^0$ band) or for a given $\Delta\ell = \pm 1$ perpendicular band (for example the $\nu_4{}^1$ band) can be written as:

$${}^1\mu_Z^{\Delta\ell=0} = {}^1\mu_0^{\Delta\ell=0} \, \varphi_z + {}^1\mu_1^{\Delta\ell=0} \, \tfrac{1}{2} \, \left\{ \varphi_x, iJ_y \right\} - \left\{ i\varphi_y, J_x \right\} + {}^1\mu_2^{\Delta\ell=0} \, \left\{ \varphi_z, J^2 \right\} + {}^1\mu_3^{\Delta\ell=0} \, \left\{ \varphi_z, J_z^2 \right\} \ldots \quad (10)$$

$${}^4\mu_Z^{\Delta\ell=1} = {}^4\mu_0^{\Delta\ell=1} \, i\varphi_y + {}^4\mu_4^{\Delta\ell=1} \, \left\{ \varphi_x, J_z \right\} + {}^4\mu_5^{\Delta\ell=1} \, \left\{ \varphi_z, J_x \right\} + \ldots \quad (11)$$

with in ($\Delta\ell=0;\Delta K=0$) and in ($\Delta\ell=\pm1;\Delta K=\pm1$) selection rules for the $\nu_1{}^0$ and $\nu_4{}^1$ bands, respectively. According to Tarrago and Delaveau [30] higher order terms in ($\Delta\ell=0;\Delta K=\pm3$) and ($\Delta\ell=\pm1;\Delta K=\mp2$) are also to be considered in the expansions given in Eqs. (10) and (11), respectively. However, these terms do not lead to any improvement for the present line intensity calculation. Finally for ($\Delta\ell=\pm2;\Delta K=\mp1$) perpendicular bands, like the $2\nu_5{}^2$ dark band, the expansion of the transformed transition dipole moment operator takes a form:

$$^{55}\mu_Z^{\Delta\ell=2} = {}^{55}\mu_1^{\Delta\ell=2}\varphi_x + \ldots, \tag{12}$$

which differs in phase factor from ($\Delta\ell=\pm1;\Delta K=\pm1$) type transitions.

In Eqs. (10-12), φ_z, φ_y and φ_z are the Z_x, Z_y and Z_z components of the direction cosines between the Z laboratory fixed axes and the x, y and z molecular axes. The elements of matrices are given in Tables VIII of Ref. [38]. As compared to Table II of Ref. [30], these dipole moment matrix elements differ only by the definition of the expansion terms for the $\nu_1{}^0$ and $\nu_4{}^1$ bands.

The $\nu_1{}^0$ and $\nu_4{}^1$ bands are fundamental bright bands, and their non-zero transition moment operators involve first order derivatives of the CH_3Cl dipole moment. On the other hand, for the $3\nu_6{}^1$, $3\nu_6{}^3$, $2\nu_5{}^2$ and $2\nu_3+\nu_5{}^1$ overtone or combination bands, the transition dipole moment operators are assumed to have negligible value since they involve second order derivatives of the dipole moment.

The goal of the present study was to explain the observed intensity pattern at 3.4 μm. In this approach the dark bands are observable because they borrow their intensities from the strong $\nu_1{}^0$ band and the medium-intensity $\nu_4{}^1$ band. To demonstrate this effect, only the parameters involved in the expansion of the $\nu_1{}^0$ and $\nu_4{}^1$ bands were considered in the line intensity calculation.

A similar theoretical approach was adopted by Dang-Nhu [10], but at that time the calculation was restricted to the $\nu_4{}^1$ and $3\nu_6{}^1$ interacting bands. Indeed in Ref. [5] the intensity calculation was performed for the $\nu_1{}^0$ band assuming that this band was isolated.

In order to increase the consistency of the intensity parameters, the experimental line intensity achieved in this work for $^{12}CH_3{}^{35}Cl$ and $^{12}CH_3{}^{37}Cl$ were introduced altogether in the

least squares fit calculation. In this way, a common set of ${}^{4}\mu_i^{\Delta\ell=1}$ and ${}^{1}\mu_i^{\Delta\ell=0}$ parameters was obtained for both isotopic species: these are collected in Table 8. Let us also mention that the sets of intensity parameters achieved from separate intensity calculations performed for $^{12}CH_3{}^{35}Cl$ and $^{12}CH_3{}^{37}Cl$ do not differ significantly within their experimental uncertainty. The statistical analysis of the line intensity calculation is given in Table 8, showing that the calculations are satisfactory. The full comparison between experimental results of Section 3 and the theoretical calculation is given as supplementary data. Table 9 gives sample of such comparisons for several $CH_3{}^{35}Cl$ and $CH_3{}^{37}Cl$ line intensities.

8. Line list for the 3.4 µm region

For atmospheric applications in the 3.4 µm region, a complete list of line positions and intensities was generated for the $\nu_1{}^0$, $\nu_4{}^1$ and $3\nu_6{}^1$ bands of both $^{12}CH_3{}^{35}Cl$ and $^{12}CH_3{}^{37}Cl$ isotopologues. This list was restricted to the 2920-3100 cm^{-1} region since the present study does not concern the weaker and highly perturbed bands located at different frequencies [12-14]. The line positions were computed using the vibrational energies together with the rotational and coupling constants of Table 5 ($^{12}CH_3{}^{35}Cl$) and Table 6 ($^{12}CH_3{}^{37}Cl$) for the upper {(v_5=2; ℓ =±2), (v_3=2,v_5=1; ℓ =±1), (v_1=1; ℓ =0), (v_4=1; ℓ =±1), (v_6=3; ℓ =±1), (v_6=3; ℓ =±3)} resonating states and of Ref. [18] for the ground state. For $CH_3{}^{35}Cl$, several perturbations due to dark states are not accounted for correctly in our calculation (see the discussion in section 6). As a consequence, the positions of $CH_3{}^{35}Cl$ lines were obtained using, whenever possible, the observed energies of the (v_5=2; ℓ =±2), (v_3=2,v_5=1; ℓ =±1), (v_1=1; ℓ =0), (v_4=1; ℓ =±1), (v_6=3; ℓ =±1), (v_6=3; ℓ =±3) upper levels. The intensities were computed using the transition dipole moment constants given in Table 8.

The line list was generated in the HITRAN format [40]. For this purpose broadening coefficients had to be introduced. Values from HITRAN08 [2] originating from Ref. [16] for the self-broadening and from Ref. [41] for the air-broadening. The line list is available on request to the authors. Table 10 provides some statistics of its content as for example the Sum of the Individual Line Intensities at 296K (SILI) obtained from line intensities of the $\nu_1{}^0$, $\nu_4{}^1$ bright bands together with those of the various dark bands $3\nu_6{}^1$, $2\nu_5{}^2$, $2\nu_3+\nu_5{}^1$ and $3\nu_6{}^3$.

The ratio of the $\nu_4{}^1$ to $\nu_1{}^0$ band has to be compared to what can be expected from the ratio of the zero order expansion of the transition dipole moment operator squared:

$$\left|{}^{4}\mu_0^{\Delta\ell=1}\right|^2 \Big/ \left|{}^{1}\mu_0^{\Delta\ell=0}\right|^2 \approx 0.53 \qquad (13)$$

This ratio differs from the $\nu_4{}^1$ to $\nu_1{}^0$ band intensity ratio:

$$^{ISO}SILI_{\nu 4}(296K)/\ ^{ISO}SILI_{\nu 1}(296K) \approx 0.42 \qquad (14)$$

with ISO=35 or ISO=37. But when considering the $3\nu_6{}^1$ and $\nu_4{}^1$ contributions, the agreement with Eq. (13) becomes excellent:

$$(^{ISO}SILI_{\nu 4}(296K)+\ ^{ISO}SILI_{3\nu 6}(296K))\ /\ ^{ISO}SILI_{\nu 1}(296K) \approx 0.54. \qquad (15)$$

Therefore, it is clear that the model accounts correctly for the intensity transfer $\nu_4{}^1 \rightarrow 3\nu_6{}^1$. The good agreement is also observable in the overall structure of the 3.4 µm region (see Fig. 1)

In addition, Figs. 2-3 and 6-8 give detailed comparisons of observed spectra in various regions. Figures 2 and 3 give portions of the $\nu_1{}^0$ band. Figures 6 and 7 show perturbed regions of the $\nu_4{}^1$ band: because of local resonances, transitions from the dark $2\nu_3+\nu_5{}^1$ and $3\nu_6{}^3$ are observable. Finally, Fig. 8 gives a portion of the *Q*- and *R*-branches of the weak and perturbed $\nu_4{}^1$ and $3\nu_6{}^1$ bands. In all spectral ranges, the agreement is excellent.

9. Comparison with existing line intensity data

As it was mentioned in the introduction the existing line intensities for the 3.4 µm bands of methyl chloride are rather sparse.

The only existing individual line intensities at 3.4 µm were delivered by Dang-Nhu and co workers [5, 10]. The experimental intensities achieved during the present work are ~(9±4)% weaker than those of Dang-Nhu et al. for the $\nu_1{}^0$ band. A summary of the comparison have been resumed in Table 11. Let us remember that only a single FTS spectrum

(P=0.0363 Torr, path length l=2012 cm) was used during Dang-Nhu investigations. On the contrary, during the present study, the CH_3Cl intensities were extracted from a large set of FTS spectra recorded in different experimental conditions (see Table 1) and using for data retrievals a software taking into account both apparatus function and broadening effects [15]. Since the linelist present in the HITRAN [2] and GEISA [3] databases at 3.4 µm originates from Dang-Nhu studies for CH_3Cl [5, 10], the individual lines generated in the present work are ~6 % weaker than those in HITRAN [2] or GEISA [3].

To our knowledge the only existing recent band intensity measurements were performed at the Pacific Northwest National Laboratory (PNNL) [11]. In order to compare our results to the measured integrated band intensities $S_{3\mu m}$(PNNL), it is necessary to account properly for the contribution of hot bands quantified as $R_{hot} \approx (Q_{Vib}(T)-1)$, where $Q_{Vib}(T)$ is the vibrational partition function (see Eq. (7)). Contributions from isotopic species differing from $^{12}CH_3{}^{35}Cl$ and $^{12}CH_3{}^{37}Cl$ have also to be taken into account through $R_{ISO} \approx 1 - I_{35} + I_{37}$.

Therefore, our estimation for the integrated band intensities is:

$$^{Calc}S_{3\mu m} \approx \frac{Q_{Vib}(296K)}{I_{35}+I_{37}} \sum_{\text{all bands}} S_{Band}(296K) \qquad (16)$$

In this expression $S_{Band}(296K)$ is the sum of all individual line intensities for a given vibrational band at 296 K.

If we compare our calculated ($^{Calc}S_{3\mu m}$) to the PNNL measured ($S_{3\mu m}$(PNNL)) integrated intensities, the ratio $R = S_{3\mu m}(PNNL)/^{Calc}S_{3\mu m}$ varies from 0.98 to 1.02, depending on the considered spectral range (see Table 12).

10. Conclusion

Using high-resolution Fourier transform spectra of natural methyl chloride, an extensive analysis of the $\nu_1{}^0$, $\nu_4{}^1$ and $3\nu_6{}^1$ bands of the $CH_3{}^{35}Cl$ and $CH_3{}^{37}Cl$ isotopic species was performed up to very high rotational quantum numbers. The upper state energy levels were calculated using a Hamiltonian matrix taking explicitly into account the interactions that couple altogether the {(v_5=2; ℓ =±2), (v_3=2,v_5=1; ℓ =±1), (v_1=1; ℓ =0), (v_4=1; ℓ =±1), (v_6=3; ℓ =±1), (v_6=3; ℓ =±3)} interacting states through Coriolis and anharmonic resonances.

The upper state parameters (band centers, rotational and coupling constants) derived in this work allow to reproduce most of the observed experimental data, within their experimental uncertainties. An extended set of individual line intensities was measured for $CH_3{}^{35}Cl$ and $CH_3{}^{37}Cl$ isotopic species and least squares fitted to get the line intensity parameters for the 3.4 µm region. Finally, a complete list of line parameters was generated for the first time in the 3.4 µm region. The line intensities delivered in this work were compared to the recent integrated intensities from PNNL. A subsequent work is in progress and will involve line shape parameters (self- and N_2-broadening coefficients) in the 3.4 µm region.

Acknowledgments

The authors gratefully acknowledge for financial support from the French LEFE-CHAT program “Les Enveloppes Fluides et l'Environnement, Chimie Atmosphérique” of the French “Institut National des Sciences de l'Univers” (INSU) of CNRS. In addition, A.P. thanks the “Centre National d'Etudes Spatiales” (CNES) for additional financial support.

References

[1] Kaley AW, Weigum N, McElcheran C, Taylor JR. Global methyl chloride measurements from the ACE-FTS instrument. International Symposium on Molecular Spectroscopy Department of Chemistry The Ohio State University, TI-09; 2009.

[2] Rothman LS, Gordon IE, Barbe A, Benner DC, Bernath PF, Birk M, Boudon V, Brown LR, Campargue A, Champion JP, Chance K, Coudert LH, Dana V, Devi VM, Fally S, Flaud JM**,** Gamache RR, Goldmanm A, Jacquemart D, Kleiner I, Lacome N, Lafferty QJ, Mandin JY, Massie ST, Mikhailenko SN, Miller CE, Moazzen-Ahmadi N, Naumenko OV, Nikitin AV**,** Orphal J, Perevalov VI, Perrin A**,** Predoi-Cross A, Rinsland CP, Rotge M, Imeckova MS, Smith MAH, Sung K, Tashkun SA, Tennyson J, Toth RA, Vandaele AC, Vander Auwera J. The HITRAN 2008 molecular spectroscopic database, JQSRT 2009;110**:**533–72.

[3] Jacquinet-Husson N, Scott NA, Chédin A, Crépeau L, Armante R, Capelle V, Orphal J, Coustenis A, Barbe A, M. Birk, Brown LR, Camy-Peyret C, Claveau C, Chance K, Christidis N, Clerbaux C, Coheur PF, Dana V, Daumont L, Debacker-Barilly MR, Di Lonardo G, Flaud JM, Goldman A, Hamdouni A, Hess M, Hurley MD, Jacquemart D, Kleiner I, Köpke P, Mandin JY, Massie S, Mikhailenko S, Nemtchinov V, Nikitin A, Newnham D, Perrin A, Perevalov VI, Pinnock S, Régalia-Jarlot L, Rinsland CP, Rublev A, Schreier F, Schult L, Smith KM, S.A. Tashkun, Teffo JL, Toth RA, Tyuterev VlG, Vander Auwera J, Varanasi P, Wagner G, The GEISA spectroscopic database: Current and future archive for Earth's planetary atmosphere studies. JQSRT 2008;109:1043-59.

[4] Morillon-Chapey M, Graner G. Fine Structure in the ν_1 Band of CH_3Cl Near 2970 cm^{-1}. J Mol Spectrosc 1969;31:155-19.

[5] Dang-Nhu M**,** Morillon-Chapey M, Graner G, Guelachvili G**.** Intensities of the ν_1 bands of $^{12}CH_3{}^{35}C1$ and $^{12}CH_3{}^{37}Cl$ near 3 μm. JQSRT 1981;26:515-521.

[6] Jensen P, S. Brodersen S, Guelachvili G. Determination of A_0 for $CH_3{}^{35}CI$ and $CH_3{}^{37}CI$ from the ν_4 Infrared and Raman Bands, J Mol Spectrosc 1981;88**:**378-93.

[7] Nikitin A. Vibrational energy levels of methyl chloride calculated from full dimensional ab initio potential energy surface. J Mol Spectrosc 2008;252:17–21.

[8] Margolis JS, Toth RA. Absorption Strength Measurement of the ν_1 band of methyl chloride. J Mol Spectrosc 1977;66:30-34.

[9] Margolis JS. Absorption Strength Measurement of the ν_4 band of methyl chloride. J Mol Spectrosc 1978;70:257-262.

[10] Dang-Nhu M**,** Morillon-Chapey M, Graner G, Guelachvili G. Intensites des raies d'absorption des bandes perturbées ν_4 et $3\nu_6$ de CH_3CI. Can J Phys 1982;60:1328-33.

[11] Sharpe SW, Johnson TJ, Sams RL, Chu PM, Rhoderick GC, Johnson PA. Gas-Phase Databases for Quantitative Infrared Spectroscopy. Appl Spectrosc 2004; 58:1452-61.

[12] Bensari-Zizi N, Alamichel C. Fermi resonance between the ν_1, and $2\nu_5{}^0$ infrared bands of methyl chloride. Mol Phys 1981;43:1255-65

[13] Bensari-Zizi N , Alamichel. C, Guelachvili G. Etude des bandes infrarouges en resonance $2\nu_2$, $\nu_2 + \nu_5$, $2\nu_5^0$, $2\nu_5^{\pm 2}$, $2\nu_3 + \nu_5$ et $4\nu_3$, du chlorure de methyle. Can J Phys 1982;60:825-43.

[14] Bensari-Zizi N, Alamichel C. Study of the $\nu_3+2\nu_6$: and $\nu_2+2\nu_3$ infrared bands of methyl chloride. Can J Phys 1982;60**:**1661.

[15] Jacquemart D, Mandin JY, Dana V, Picqué N, Guelachvili G. A multispectrum fitting procedure to deduce molecular line parameters. Application to the 3-0 band of $^{12}C^{16}O$. Eur Phys J D 2001;14:55-69.

[16] Chackerian C, Jr, Brown LR, Lacome N, Tarrago G. Methyl Chloride ν_5 Region Lineshape Parameters and Rotational Constants for the ν_2, ν_5, and $2\nu_3$ Vibrational Bands. J Mol Spectrosc 2008;191:148-57.

[17] Dana V, Mandin JY. New improvements in the determination of line parameters from FTS data. JQSRT 1992;4:725-31.

[18] Nikitin A, Champion JP. New ground state constants of $^{12}CH_3{}^{35}Cl$ and $^{12}CH_3{}^{37}Cl$ from global polyad analysis. J Mol Spectrosc 2005;230:168–73.

[19] Nikitin A, Champion JP, Bürger H. Global analysis of $^{12}CH_3{}^{35}Cl$ and $^{12}CH_3{}^{37}Cl$: simultaneous fit of the lower five polyads (0–2600 cm^{-1}). J Mol Spectrosc 2005;230:174–84.

[20] Constantin FL, Demaison J, Féjard L, Litz M, Bürger H, Pracna P. High-resolution infrared and subterahertz spectroscopy of the $\nu_2 = 1$, $\nu_5 = 1$, and $\nu_3 = 2$ levels of $^{13}CH_3{}^{35}Cl$. J Mol Spectrosc 2007;243:234-44.

[21] Nikitin A, Féjard L, Champion JP, Bürger H, Litz M, Colmont JM, Bakri B. New measurements and global analysis of chloromethane in the region from 0 to 1800 cm^{-1}. J Mol Spectrosc 2003;221:199-212.

[22] Bensari-Zizi N, Guelachvili G, Alamichel C. Etude de la bande $\nu_2+ \nu_3$ de CH_3CI en résonance de Coriolis avec $\nu_3 + \nu_5$. Mol Phys 1977;34:1131-40.

[23] Bensari-Zizi N, Alamichel C,. Guelachvili G. Etude de la bande $\nu_2 + \nu_3$ de CH_3CI en resonance de Coriolis avec $\nu_3 +\nu_5$. Mol Phys 1982;46:171-175.

[24] Di Lauro C, Alamichel C. Rotational analysis of the $\nu_2+\nu_6$, $\nu_5+\nu_6$, $\nu_5+\nu_6$ and $2\nu_3+\nu6$ interacting infrared bands of methyl chloride. J Mol Spectrosc 1980;81:390-412.

[25] Pracna P, Sarka K, Demaison J, Cosléou J, Herlemont F, Khelkhal M, Fichoux H, Papousek D, Paplewski M, Bürger H. High-Resolution Study of the ν_5 =1 Level of CDF_3, J Mol Spectrosc 1997;184**:**93–105.

[26] Bürger H, Cosléou J, Demaison J, Gerke C, Harder H, Mäder H, Paplewski M, Papousek D, Sarka K, Watson JKG. Radiofrequency, Microwave, Submillimeter-Wave, and High-Resolution Infrared Spectra of the ν_6 =1 Vibrational State of CDF_3. J Mol Spectrosc 1997;182**:**34–49.

[27] Sarka K, Papousek D, Demaison J, Mäder H, Harder H. Vibration–Rotational Spectroscopy and Molecular Dynamics. In D.Papousek, Ed., Vol. 9, Advances in Physical Chemistry, World Scientific, Singapore; 1997.

[28] Kwabia Tchana F, Kleiner I, Orphal J, Lacome N, Bouba O. New analysis of the Coriolis-interacting ν_2 and ν_5 bands of $CH_3{}^{79}Br$ and $CH_3{}^{81}Br$. J Mol Spectrosc 2004;228:441-52.

[29] Tarrago G. The frequencies of vibration-rotation transitions of molecules with ternary axis of symmetry; calculation of the corrections to fourth order. Cah Phys 1965;19:149-217.

[30] Tarrago G, Delaveau M. Triad $\nu,(A,)$, $\nu_t(E)$, $\nu_f(E)$ in C_{3v} Molecules: Energy and Intensity Formulation (Computer Programs). J Mol Spectrosc 1986;119:418-25.

[31] Fusina L, Di Lonardo G. The ν_2 and ν_4 bending fundamentals of phosphine (PH_3). J Mol Struct 200;517-518:67-78.

[32] Pracna P, Müller HSP, Urban Š, Horneman VM, Klee S. Interactions between vibrational polyads of propyne, $H_3C\_C{\equiv}CH$: Rotational and rovibrational spectroscopy of the levels around 1000 cm^{-1}. J Mol Spectrosc 2009;256 :152–62.

[33] Pracna P, Ceausu-Velcescu A, Predoi-Cross A, Š Urban Š. Rovibrational spectroscopy of the Fermi-interacting $\nu_4 = 1$ and $\nu_3 = \nu_6 = 1$ levels of DCF_3. J Mol Spectrosc 2010;259:1–10.

[34] Wötzel H, Mäder H, Harder H**,** Pracna P, Sarka K. The direct l-type resonance spectrum of CF_3CCH in the vibrational state ν_{10}=3: Extension of the theory of reduction to H_{6n} terms. J Mol Struct 2006;780-81:206-21.

[35] Najib H, Bensari-Zizi N, Bürger H, Guelachvili G, Alamichel C. Anharmonic resonances between the upper rovibrational levels of the $\nu_2+\nu_4^{\pm1}$, $\nu_2+3\nu_6^{\pm1}$, $\nu_1+\nu_5^{\pm1}$, $3\nu_5^{\pm1}$, $\nu_4^{\pm1}+\nu_5^{\pm1}$, $\nu_5^{\pm1}+3\nu_6^{\pm1}$, $\nu_5^{\pm1}+3\nu_6^{\pm3}$ and $2\nu_3+3\nu_6^{\pm1}$ infrared bands of $CH_3{}^{35}Cl$ studied in a high-resolution FTIR spectrum from 4250 to 4600 cm^{-1}. Mol Phys 1990;70:849-62.

[36] De Bievre P, Holden NE, Barnes IL. Isotopic Abundances and Atomic Weights of the Elements. J Phys Chem Ref Data 1984;13:809-91.

[37] Fischer J, Gamache RR, Goldman A, Rothman LS, Perrin A. Total internal partition sums for molecular species in the 2000 edition of the HITRAN database. JQSRT 2003;82:401–12.

[38] Flaud JM, Camy-Peyret C, Toth RA. Water Vapour Line Parameters from Microwave to Medium Infrared. Pergamon press, Oxford; 1981.

[39] Brown LR, Sams RL, Kleiner I, Cottaz C, Sagui L. Line Intensities of the Phosphine Dyad at 10 μm. J Mol Spectrosc 2002;215(2):178-203.

[40] Rothman LS, Jacquemart D, Barbe A, Benner DC, Birk M, Brown LR, Carleer MR, Chackerian Jr C, Chance K, Coudert LH, Dana V, Devi VM, Flaud JM, Gamache RR, Goldman A, Hartmann JM, Jucks KW, Maki AG, Mandin JY, Massie ST, Orphal J, Perrin A, Rinsland CP, Smith MAH, Tennyson J, Tolchenov RN, Toth RA, Vander Auwera J, Varanasi P, Wagner G. The HITRAN 2004 molecular spectroscopic database. JQSRT 2005;96:139-204.

[41] Bouanich JP, Blanquet G, Walrand J. Theoretical O_2- and N_2-Broadening Coefficients of CH_3Cl Spectral Lines. J Mol Spectrosc 1993;161:416-26.

Table captions

Table 1:

Experimental conditions and characteristics of the recorded spectra.

Table 2:

(A) Energy levels analysis of the 3.4 μm region.

(B) Statistical analysis of the energy level calculations.

Table 3:

Vibrational modes for $CH_3{}^{35}Cl$ and $CH_3{}^{37}Cl$.

Table 4:

Hamiltonian matrix used to describe the {(v_5=2; ℓ =±2), (v_3=2, v_5=1; ℓ =±1), (v_1=1; ℓ =0), (v_4=1; ℓ =±1), (v_6=3; ℓ =±1), (v_6=3; ℓ =±3)} resonating states of methyl chloride.

Table 5:

Vibrational energies, rotational and interaction constants for the ground state and the {(v_5=2; ℓ =±2), (v_3=2,v_5=1; ℓ =±1), (v_1=1; ℓ =0), (v_4=1; ℓ =±1), (v_6=3; ℓ =±1), (v_6=3; ℓ =±3)} vibrational states of $CH_3{}^{35}Cl$ methyl chloride. All parameters are in cm^{-1}. The quoted errors are one standard deviation.

(A) Vibrational band centers and rotational constants.

(B) Interaction parameters for $CH_3{}^{35}Cl$.

Table 6:

Vibrational energies, rotational and interaction constants for the ground state and the {(v_5=2; ℓ =±2), (v_3=2,v_5=1; ℓ =±1), (v_1=1; ℓ =0), (v_4=1; ℓ =±1), (v_6=3; ℓ =±1), (v_6=3; ℓ =±3)} vibrational states of $CH_3{}^{37}Cl$ methyl chloride. All parameters are in cm^{-1}. The quoted errors are one standard deviation.

(A) Vibrational band centers and rotational constants.

(B) Interaction parameters for $CH_3{}^{37}Cl$.

Table 7:

Example of resonances observed and modeled in this work.

Table 8:

Transition moment constants for the $\nu_1{}^0$ and $\nu_4{}^1$ bands.

Table 9:

Sample of experimental measurements of line parameters obtained around 3.4 μm**.**

Table 10:

Description of the generated linelist.

Table 11:

Comparison between our measurements of line intensities with those of Dang et al. [5].

Table 12:

Comparison of the integrated intensities from PNNL and this work for various integration ranges.

Figure captions

Figure 1:

Overview of the ν_1^0, ν_4^1 and $3\nu_6^1$ band of methyl chloride in the 3.4 µm region. In the 2920-3150 cm^{-1} spectral region, the agreement of the present calculation (upper panel) with the observation (spectrum #3) is significantly improved as compared to the one obtained when using the linelist available in HITRAN [2] or GEISA [3] (lower panel). The present study does not concern the highly perturbed $2\nu_5^0$ band centered near 2880 cm^{-1}.

Figure 2:

Part of spectrum #3 near 2965 cm^{-1}. The strong ${}^{Q}Q_K$ ($\Delta J = 0$, $\Delta K=0$) series of the ν_1^0 band for K=1 to K=10 is indicated on the lower trace. All traces have the same vertical scale but are shifted for visual clarity.

Figure 3:

Part of the ${}^{Q}P$ branch of the ν_1^0 band in spectrum #3 near 2940 cm^{-1}. For K=0 the upper J' values are given and the transitions for $CH_3{}^{35}Cl$ and $CH_3{}^{37}Cl$ are marked by diamonds and triangles, respectively. All traces have the same vertical scale but are shifted for visual clarity.

Figure 4:

Single channel spectra of CH_3Cl around 3000 cm^{-1}. The upper panel corresponds to spectrum #3 recorded without any optical filter (H_2O and CO_2 transitions are observed). The bottom panel corresponds to spectrum #4 recorded with an optical filter.

Figure 5:

Example of the simultaneous fit of two transitions from 6 experimental spectra (from lower to higher pressure, see Table 1) between 2931.18 and 2931.34 cm^{-1}.

Figure 6:

Part of the methyl chloride spectrum near 2983 cm^{-1} (R branch of the ν_1^0 band). The assignments are given for $CH_3{}^{35}Cl$ (circles) and $CH_3{}^{37}Cl$ (triangles). Because of a local

resonance the forbidden $2\nu_3+\nu_5^1$ for $CH_3{}^{35}Cl$ [19 6 ← 19 5] (star) becomes observable. All traces have the same vertical scale but are shifted for visual clarity.

Figure 7:

Part of the methyl chloride spectrum near 3015 cm^{-1}: The lines of the ${}^{K'=2,\ell'=-1}Q_{K''=-3}(J)$ series of the ν_4^1 band are clearly perturbed near $J'\sim21$. As a result, the $3\nu_6^3$ [21 0← 21 3] transition is clearly observable. For both series of assigned lines, the upper state J' values are indicated. All traces have the same vertical scale but are shifted for visual clarity.

Figure 8:

Part of the methyl chloride spectrum near 3150 cm^{-1} (${}^RQ_K$ branch of the ν_4^1 band). Lines from the $3\nu_6^1$ band are also observable. All traces have the same vertical scale but are shifted for visual clarity.

Figure 9:

Analysis of the resonances perturbing the (v_4=1; ℓ =±1) energy levels for J =21 and Γ=A_1 or A_2 symmetry. The mixing coefficient % (A_1, (v_4=1; ℓ =±1), J '=21 K '| v ℓ), in percentage (see text) on the (v_6=3; ℓ =±1), (v_6=3; ℓ =±3) and (v_0=1; ℓ =0) interacting vibrational states. There exists a local resonance coupling together (v_4=1; ℓ =±1), K=-2 ⇔ (v_6=3; ℓ =±3) K=0.

Table 1:

Experimental conditions and characteristics of the recorded spectra.

Unapodized apparatus function

Nominal aperture radius	0.75 mm
Effective aperture radius	0.80 mm
Collimator focal length	418 mm

Absorbing sample

Natural CH_3Cl	74.89 % of $^{12}CH_3{}^{35}Cl$
	23.94 % of $^{12}CH_3{}^{37}Cl$
Stated purity	99.9 %

Experimental conditions

Absorption path	30.00 ± 0.05 cm
S/N ratio	≈ 700-1000

#	CH_3Cl pressure (mbar)	Resolution[a] (cm^{-1})	Number of co added scans
1	0.542	0.008	400
2	0.621	0.008	100
3[b]	0.702	0.008	400
4	1.51	0.008	400
5	3.30	0.01	400
6	7.10	0.01	237

[a] Resolution as defined by Bruker = 0.9/Maximum optical path difference.
[b] For this spectrum no optical filter has been used (see text).

Table 2:
(A) Range of observed energy levels during the analysis of the 3.4 μm of $CH_3{}^{35}Cl$ and $CH_3{}^{37}Cl$.

$CH_3{}^{35}Cl$

	$\nu_1{}^0$	$\nu_4{}^1$	$3\nu_6{}^1$	$2\nu_3+\nu_5{}^1$ (dark)	$3\nu_6{}^3$ (dark)
Number of lines	1208	1649	585	3	6
Max J, $\|K\|$	$J\leq48$, $\|K\| \leq12$	$J\leq43$, $\|K\| \leq13$	$J\leq34$, $\|K\| \leq13$	J=19, K=6	J=21 and 22, K=0
Number of levels *	584/582	720/571	271/271	1/1	2/2

$CH_3{}^{37}Cl$

	$\nu_1{}^0$	$\nu_4{}^1$	$3\nu_6{}^1$	$2\nu_3+\nu_5{}^1$ (dark)
Number of lines	712	559	98	2
Max J, $\|K\|$	$J\leq41$, $\|K\| \leq9$	$J\leq35$, $\|K\| \leq10$	$J\leq25$, $\|K\| \leq7$	J=21, K=7
Number of levels *	351/351	277/277	62/62	1/1

(B) Statistical analysis of the energy level calculations.

	$CH_3{}^{35}Cl$	$CH_3{}^{37}Cl$
Number of levels*	1578/1428	698/698
$0 \le \delta < 1.10^{-3}\ cm^{-1}$	47.8 %	61.5%
$1.10^{-3} \le \delta < 4.10^{-3}\ cm^{-1}$	41.8 %	31.8%
$4.10^{-3} \le \delta < 30.10^{-3}\ cm^{-1}$	10.4 %	6.7 %
Standard deviation (in cm^{-1})	0.34×10^{-2}	0.23×10^{-2}

* N_{Obs}/N_{Fitted} where N_{Obs} and N_{Fitted} are the number of observed levels and the number of levels used in our calculation, respectively.

$$\delta = \left|E_{obs} - E_{calc}\right|$$

Table 3:

Vibrational modes for $CH_3{}^{35}Cl$ and $CH_3{}^{37}Cl$.

Band	Sym		(1)	$CH_3{}^{35}Cl$	$CH_3{}^{37}Cl$	Ref
$\nu_1{}^0$	A_1	CH_3 stretch	E_v	2967.7691	2967.7469	This work
$\nu_2{}^0$	A_1	CH_3 bend	E_v	1354.8811	1354.6824	[19]
$\nu_3{}^0$	A_1	CCl stretch	E_v	732.8422	727.0295	[19]
$\nu_4{}^1$	E	CH_3 stretch	E_v	3039.2635	3039.6311	This work
			ν	3037.1416	3036.7516	This work
$\nu_5{}^1$	E	CH_3 bend	E_v	1452.1784	1452.1552	[19]
$\nu_6{}^1$	E	CH_3 rock	E_v	1018.0709	1017.6824	[19]
$3\nu_6{}^1$	E		E_v	3042.8944	3041.2568	This work
			ν	3045.0164	3044.1363	This work

(1) : Vibrational energies (E_v) and band center (ν) in cm^{-1}.

Table 4:

Hamiltonian matrix used to describe the {(v_5=2; ℓ =±2), (v_3=2, v_5=1; ℓ =±1), (v_1=1; ℓ =0), (v_4=1; ℓ =±1), (v_6=3; ℓ =±1), (v_6=3; ℓ =±3)} resonating states of methyl chloride.

	(v_5=2; ℓ =±2)	(v_3=2,v_5=1; ℓ =±1)	(v_1=1; ℓ =0)	(v_4=1; ℓ =±1)	(v_6=3; ℓ =±1)	(v_6=3; ℓ =±3)
(v_5=2; ℓ =±2)	**W(v; ℓ =±2)**		c.c.			
(v_3=2,v_5=1; ℓ =±1)		**W(v; ℓ =±1)**	c.c.			
(v_1=1; ℓ =0)	(±2; ∓ 1) (±2;±2)	(±1;±1)	**W(v; ℓ =0)**	c.c.	c.c.	
(v_4=1; ℓ =±1)			(±1;±1) (±1; ∓ 2)	**W(v; ℓ =±1)**	c.c.	c.c.
(v_6=3; ℓ =±1)			(±1;±1)	C(0;0) +Anh(0;0)	**W(v; ℓ =±1)**	c.c.
(v_6=3; ℓ =±3)				(±2;±2)	(±2; ∓ 1) (±2;±2)	**W(v; ℓ =±3)**

The W(v;± ℓ) are diagonal in v- rotational operators, including both diagonal and non diagonal in ℓ terms. The (±1;±1), (±1; ∓ 2), (±2:±2), and (±2; ∓ 1) are for ($\Delta\ell$;ΔK) rotational operators. *C*(0;0) and *Anh*(0;0) are for ($\Delta\ell$;ΔK)=(0;0) z-type Coriolis and Anharmonic rotational operators. See Appendix for the details of the Hamiltonian equations. c.c. corresponds to the conjugate complex.

Tables 5:
Vibrational energies, rotational and interaction constants for the ground state and the {(v_5=2; ℓ =±2), (v_3=2,v_5=1; ℓ =±1), (v_1=1; ℓ =0), (v_4=1; ℓ =±1), (v_6=3; ℓ =±1), (v_6=3; ℓ =±3)} vibrational states of $CH_3{}^{35}Cl$ methyl chloride. All parameters are in cm^{-1}. The quoted errors are one standard deviation.

(A) Vibrational band centers and rotational constants.

	$\|0\rangle$ [a]	(v_5=2; ℓ =±2)	(v_3=2,v_5=1; ℓ =±1)	(v_1=1; ℓ =0)	(v_4=1; ℓ =±1)	(v_6=3; ℓ =±1)	(v_6=3; ℓ =±3)
E_v	0	2895.566(30)	2907.903(45)	2967.7691(41)	3039.26354(640)	3042.8944(69)	3060.0064(32)
$(A\zeta)$		-1.2581523(110)	-1.3048006(110)		0.388678(490)	1.276675(750)	1.276675[b]
$c^2_{21,xz}\times10^6$					2.201(670)		
$q^1_{22}\times10^4$						-0.99398(510)	
$q^2_{22}\times10^5$						-1.485(450)	
A	5.2053361	5.212437(510)	5.43872(180)	5.149695(170)	5.179097(190)	5.282501(270)	5.09116(130)
B	0.44340278	0.4473610(790)	0.3913975(700)	0.4430333(540)	0.4435246(390)	0.4385771(120)	0.4395633(620)
$D_K\times10^5$	8.2965	[a]	[a]	7.761(103)	8.718(100)	[a]	[a]
$D_{JK}\times10^6$	6.358	[a]	[a]	6.369(260)	6.943(260)	[a]	[a]
$D_J\times10^7$	6.0381	[a]	[a]	5.426(213)	6.342(120)	[a]	[a]
$H_K\times10^9$	1.040	[a]	[a]	[a]	[a]	[a]	[a]
$H_{KJ}\times10^{10}$	3.33	[a]	[a]	[a]	[a]	[a]	[a]
$H_{JK}\times10^{11}$	1.143	[a]	[a]	[a]	[a]	[a]	[a]
$H_J\times10^{13}$	-2.99	[a]	[a]	[a]	[a]	[a]	[a]

[a] : fixed to the values of the ground state from Ref. [18].

[b] : fixed to the (v_6=3 ; ℓ =1) value.

(B) Interaction parameters for $CH_3{}^{35}Cl$.

Energy state	Energy state	$\Delta\ell$	ΔK	Constants	Values
(v_4=1; ℓ =±1)	(v_5=2; ℓ =±2)	±1	±1	C_x^1	-1.306(170)×10^{-1}
(v_4=1; ℓ =±1)	(v_5=2; ℓ =±2)	±1	±1	C_{yz}^1	-7.327(570)×10^{-3}
(v_1=1; ℓ =0)	(v_5=2; ℓ =±2)	±2	±2	Q_{22}^0	-3.949(275)×10^{-4}
(v_1=1; ℓ =0)	(v_5=2; ℓ =±2)	±2	∓1	$C_{21,y}^1$	1.3261(730)×10^{-1}
(v_1=1; ℓ =0)	(v_5=2; ℓ =±2)	±2	∓1	$C_{21,y}^2$	-1.206(270)×10^{-5}
(v_4=1; ℓ =±1)	(v_1=1; ℓ =0)	±1	±1	C_x^1	2.983(810)×10^{-2}
(v_4=1; ℓ =±1)	(v_1=1; ℓ =0)	±1	±1	C_{yz}^1	2.830(500)×10^{-3}
(v_4=1; ℓ =±1)	(v_1=1; ℓ =0)	±1	±1	C_x^2	-4.63(100)×10^{-6}
(v_4=1; ℓ =±1)	(v_1=1; ℓ =0)	±1	∓2	C_{12}^2	-6.88(130)×10^{-6}
(v_4=1; ℓ =±1)	(v_1=1; ℓ =0)	±1	∓2	C_{12}^1	1.194(110)×10^{-4}
(v_6=3; ℓ =±1)	(v_4=1; ℓ =±1)	0	0	Anh^0	3.49386(260)
(v_6=3; ℓ =±1)	(v_4=1; ℓ =±1)	0	0	Anh^1	-2.476(110)×10^{-4}
(v_6=3; ℓ =±1)	(v_4=1; ℓ =±1)	0	0	C_z^1	4.215(140).10^{-2}
(v_6=3; ℓ =±1)	(v_4=1; ℓ =±1)	0	0	C_z^2	-9.33(110)×10^{-5}
(v_1=1; ℓ =0)	(v_5=1; ℓ =±2)	±2	±2	Q_{22}^0	-3.949(270)×10^{-4}
(v_1=1; ℓ =0)	(v_3=2,v_5=1; ℓ =±1)	±1	±1	C_x^1	-6.59(160)×10^{-3}
(v_1=1; ℓ =0)	(v_3=2,v_5=1; ℓ =±1)	±1	±1	C_x^2	9.64(320)×10^{-5}
(v_6=3; ℓ =±1)	(v_1=1; ℓ =0)	±1	±1	C_x^1	2.22(130)×10^{-2}
(v_6=3; ℓ =±1)	(v_1=1; ℓ =0)	±1	±1	C_{yz}^1	5.445(610)×10^{-3}
(v_6=3; ℓ =±3)	(v_6=3; ℓ =±1)	±2	±2	$Q_{22}^{\ell=3,\ell=1}$	-0.99398×10^{-4} [c]
(v_6=3; ℓ =±3)	(v_6=3; ℓ =±1)	±2	∓1	$C_{21,xz}^1$	-4.062(640)×10^{-3}

[c]: $Q_{22}^{\ell=3,\ell=1} = q_{22}^1$ $v_6 = 1; \ell = 1$.

Tables 6:

Vibrational energies, rotational and interaction constants for the ground state and the {(v_5=2; ℓ =±2), (v_3=2,v_5=1; ℓ =±1), (v_1=1; ℓ =0), (v_4=1; ℓ =±1), (v_6=3; ℓ =±1), (v_6=3; ℓ =±3)} vibrational states of $CH_3{}^{37}Cl$ methyl chloride. All parameters are in cm^{-1}. The quoted errors are one standard deviation.

(A) Vibrational band centers and rotational constants.

	$\|0\rangle$ [a]	(v_5=2; ℓ =±2)	(v_3=2,v_5=1; ℓ =±1)	(v_1=1; ℓ =0)	(v_4=1; ℓ =±1)	(v_6=3; ℓ =±1)	(v_6=3; ℓ =±3)
E_V		2895.449(160)	2893.7394(2)	2967.74693(48)	3039.6311(500)	3041.2569(500)	3058.69130(780)
$(A\zeta)$		-1.24096(330)	-1.30462465(17)		0.384630(370)	1.281021(300)	1.281021 [b]
$q_{22}^1 \times 10^4$						-1.2917(430)	
$\eta_J \times 10^5$					-3.233(130)		
A	5.205374000	5.17794(620)	5.092566(150)	5.1499699(520)	5.179460(100)	5.282427(180)	4.21495(170)
B	0.4365742400	0.440932(810)	0.4302316(190)	0.435455(290)	0.43671050(750)	0.4318326(130)	0.4343297(230)
$D_K \times 10^5$	8.427500000	[a]	[a]	8.169(100)	[a]	[a]	[a]
$D_{JK} \times 10^6$	6.449200000	[a]	[a]	[a]	[a]	[a]	[a]
$D_J \times 10^7$	5.859980000	[a]	[a]	[a]	[a]	[a]	[a]
$H_K \times 10^9$	8.340	[a]	[a]	[a]	[a]	[a]	[a]
$H_{KJ} \times 10^{10}$	2.83	[a]	[a]	[a]	[a]	[a]	[a]
$H_{JK} \times 10^{11}$	9.58	[a]	[a]	[a]	[a]	[a]	[a]
$H_J \times 10^{13}$	-3.14	[a]	[a]	[a]	[a]	[a]	[a]

[a] : fixed to the values of the ground state from Ref. [18].

[b] : fixed to the (v_6=3 ; ℓ =1) value.

(B) Interaction parameters for $CH_3{}^{37}Cl$.

Energy state	Energy state	$\Delta\ell$	ΔK	Constants	Values
(v_6=3; ℓ =±3)	(v_6=3; ℓ =±1)	±2	±2	$Q_{22}^{\ell=3,\ell=1}$	-0.8212(310)×10^{-4}
(v_6=3; ℓ =±3)	(v_6=3; ℓ =±1)	±2	±2	$F_{22,K}^{\ell=3,\ell=1}$	4.444(280)×10^{-6}
(v_1=1; ℓ =0)	(v_3=2,v_5=1; ℓ =±1)	±1	±1	C_x^1	-9.646(190)×10^{-2}
(v_1=1; ℓ =0)	(v_3=2,v_5=1; ℓ =±1)	±1	±1	C_x^2	-7.983(670)×10^{-6}
(v_1=1; ℓ =0)	(v_3=2,v_5=1; ℓ =±1)	±1	±1	C_{yz}^1	-7.401(150)×10^{-3}
(v_1=1; ℓ =0)	(v_5=2; ℓ =±2)	±2	∓1	$C_{21,y}^1$	2.020(240)×10^{-1}
(v_1=1; ℓ =0)	(v_5=2; ℓ =±2)	±2	∓1	$C_{21,y}^2$	-6.79(190)×10^{-6}
(v_1=1; ℓ =0)	(v_5=1; ℓ =±2)	±2	±2	Q_{22}^0	-3.377(110)×10^{-4}
(v_6=3; ℓ =±1)	(v_4=1; ℓ =±1)	0	0	C_z^1	-6.90(120)×10^{-2}
(v_6=3; ℓ =±1)	(v_4=1; ℓ =±1)	0	0	C_z^2	4.22(180)×10^{-5}
(v_6=3; ℓ =±3)	(v_4=1; ℓ =±1)	±2	∓1	$C_{21,xz}^1$	-6.826(340)×10^{-3}
(v_6=3; ℓ =±3)	(v_4=1; ℓ =±1)	±2	∓1	$C_{21,y}^2$	-2.287(220)×10^{-5}
(v_6=3; ℓ =±1)	(v_1=1; ℓ =0)	±1	±1	C_x^1	7.004(870)×10^{-2}
(v_6=3; ℓ =±1)	(v_1=1; ℓ =0)	±1	±1	C_x^2	-2.56(190)×10^{-6}
(v_6=3; ℓ =±1)	(v_1=1; ℓ =0)	±1	±1	C_{yz}^1	8.695(500)×10^{-3}
(v_6=3; ℓ =±1)	(v_4=1; ℓ =±1)	0	0	Anh^0	3.6018(110)
(v_6=3; ℓ =±1)	(v_4=1; ℓ =±1)	0	0	Anh^1	1.669(300)×10^{-3}
(v_6=3; ℓ =±1)	(v_4=1; ℓ =±1)	0	0	Anh^2	-2.804(300)×10^{-4}
(v_4=1; ℓ =±1)	(v_1=1; ℓ =0)	±1	±1	C_{yz}^1	3.529(350)×10^{-3}
(v_4=1; ℓ =±1)	(v_1=1; ℓ =0)	±1	±1	C_x^1	-2.006(340)×10^{-2}
(v_4=1; ℓ =±1)	(v_1=1; ℓ =0)	±1	±1	C_x^2	-6.10(100)×10^{-6}
(v_4=1; ℓ =±1)	(v_1=1; ℓ =0)	±1	±1	C_{yz}^2	-2.350(190)×10^{-5}

Table 7:

Example of resonances observed and modeled in this work.

$CH_3{}^{35}Cl$								
Symmetry		*K* values			*K* values	Type	Max %	*J* Max
A_1, A_2	(v_1=1; ℓ =0)	9	↔	(v_4=1; ℓ =±1)	8	slow	50%	43
E	(v_1=1; ℓ =0)	-5	↔	(v_3=2, v_5=1; ℓ =±1)	6	sharp	30%	19
A_1, A_2	(v_6=3; ℓ =±1)	-2	↔	(v_6=3; ℓ =±3)	0	slow	37%	21
E	(v_1=1; ℓ =0)	1,-2,4,-5,8	↔	(v_5=2; ℓ =±2)	0,-1,2,3,-3	slow	≤9%	all *J*
A_1, A_2	(v_1=1; ℓ =0)	12	↔	(v_6=3; ℓ =±1)	-13	slow	45%	45
A_1, A_2, E	(v_4=1; ℓ =±1)	all	↔	(v_6=3; ℓ l=±1)	all	strong	≤50%	all *J*

$CH_3{}^{37}Cl$								
A_1, A_2	(v_1=1; ℓ =0)	9	↔	(v_6=3; ℓ =±1)	8	slow	17%	48
A_1, A_2	(v_1=1; ℓ =0)	6	↔	(v_3=2, v_5=1; ℓ =±1)	7	sharp	34%	21
A_1, A_2	(v_6=3; ℓ =±1)	-2	↔	(v_6=3; ℓ =±3)	0	slow	49%	48
E	(v_1=1 ℓ =0)	1,-2,4,-5,8	↔	(v_5=2; ℓ =±2)	0,-1,2,3,-3	slow	4%	48
A_1, A_2	(v_1=1; ℓ =0)	12	↔	(v_6=3; ℓ =±1)	-13	slow	45%	45
A_1, A_2, E	(v_6=3; ℓ =±1)	all	↔	(v_6=3; ℓ =±1)	all	strong	≤50%	all *J*

Table 8:

Transition moment constants for the $\nu_1{}^0$ and $\nu_4{}^1$ bands.

Band	Constants		Value in Debye
$\nu_1{}^0$	${}^1\mu_0^{\Delta\ell=0}$	φ_z	$0.524519(660)\times10^{-1}$
	${}^1\mu_1^{\Delta\ell=0}$	$\frac{1}{2}\ \varphi_x, \mathrm{i}J_y\ -\ \mathrm{i}\varphi_y, J_x$	$-0.1697(290)\times10^{-4}$
$\nu_4{}^1$	${}^4\mu_0^{\Delta\ell=1}$	$\mathrm{i}\varphi_y$	$0.37475(150)\times10^{-1}$
	${}^4\mu_4^{\Delta\ell=1}$	φ_x, J_z	$-0.1849(230)\times10^{-3}$
	${}^4\mu_5^{\Delta\ell=1}$	φ_z, J_x	$-0.7075(570)\times10^{-4}$

φ_x, φ_y and φ_z stands for the direction cosines Φ_{Zx} , Φ_{Zy} and Φ_{Zz} , respectively. The transition moment constants are given in Debye (1 Debye =3.22564×10^{-30} C.m) and the quoted errors are one standard deviation.

Statistical analysis for the line intensity calculation:

	$CH_3{}^{35}Cl$	$CH_3{}^{37}Cl$
Number of lines	181	375
Percentage of lines		
$0\le\delta<8\%$	73.1%	74.9%
$8\%\le\delta<16\%$	16.0%	17.2%
$16\%\le\delta<40\%$	10.9%	7.9%

$$\delta = 100\times\left|I_{Obs} - I_{Calc}\right| / I_{Obs}$$

Table 9:

Sample of experimental measurements of line parameters obtained around 3.4 μm**.**

*	Assignment								Position	Diff	S_{obs}	S_{calc}	%
	ISO	Band	Upper state			Lower state							
	241	v1-0	37	6	A	38	6	A	2932.3536	-0.220	0.303E-01	0.298E-01	1.7
	241	v1-0	38	4	E	39	4	E	2932.5665	-0.230	0.258E-01	0.211E-01	18.2
	241	v1-0	38	3	A	39	3	A	2932.9437	-0.010	0.462E-01	0.501E-01	-8.4
	241	v1-0	37	-5	E	38	-5	E	2932.9551	0.170	0.196E-01	0.195E-01	0.4
	242	v1-0	38	4	E	39	4	E	2933.0720	0.740	0.238E-01	0.201E-01	15.9
	241	v1-0	38	-2	E	39	-2	E	2933.1944	-0.110	0.289E-01	0.281E-01	2.5
	242	v1-0	14	0	A1	13	0	A2	2979.9795	0.000	0.221E+00	0.221E+00	0.0
	242	v1-0	16	-5	E	15	-5	E	2980.3384	-0.410	0.110E+00	0.113E+00	-3.1
	242	v1-0	15	3	A	14	3	A	2980.3526	-0.210	0.339E+00	0.348E+00	-2.9
	241	v1-0	21	10	E	20	10	E	2980.8805	-0.800	0.170E-01	0.147E-01	13.6
	242	v1-0	16	-2	E	15	-2	E	2981.5030	0.230	0.212E+00	0.201E+00	5.4
	242	v1-0	19	7	E	18	7	E	2981.6295	-0.180	0.665E-01	0.599E-01	10.0
	242	v1-0	17	4	E	16	4	E	2981.7112	-0.280	0.142E+00	0.145E+00	-2.5
	242	3v6-1	20	0	E	20	1	E	3031.2429	1.600	0.257E-01	0.228E-01	11.2
	242	v4-1	12	0	E	12	1	E	3031.7407	-0.330	0.333E-01	0.291E-01	12.8
	242	v4-1	11	-1	E	10	-2	E	3033.2274	0.010	0.130E-01	0.987E-02	23.8
	242	v4-1	23	2	E	24	1	E	3033.2468	2.050	0.183E-01	0.176E-01	3.6
	242	v4-1	14	1	A1	15	0	A2	3033.4778	1.260	0.334E-01	0.311E-01	7.1
	242	v4-1	13	1	A2	14	0	A1	3034.4171	1.970	0.314E-01	0.300E-01	4.2
	242	v4-1	13	4	A	12	3	A	3082.5827	-1.770	0.587E-01	0.601E-01	-2.3
	242	v4-1	14	4	A	13	3	A	3083.4206	-1.750	0.608E-01	0.596E-01	2.0
	242	v4-1	7	5	E	6	4	E	3085.8126	-0.190	0.469E-01	0.469E-01	0.1
*	242	v4-1	27	-3	E	26	-2	E	3085.8136	-1.190			

In Column 1, "241" and "242" refer to the $CH_3{}^{35}Cl$ and $CH_3{}^{37}Cl$ isotopic species, respectively (HITRAN notation). Column 2 gives assignment for the upper vibrational states (v1-0, v4-1 and 3v6-1 stand for (v_1=1; ℓ=0), (v_4=1; ℓ=1) and (v_6=3; ℓ=1), respectively). Columns 3 to 8 give the upper and lower *J*, *K* rotational quantum numbers and symmetry types. Note that "A" stands for overlapping $A_1 \leftarrow A_2$ and $A_2 \leftarrow A_1$ transitions. Columns 9 and 10 give the calculated line positions (in cm^{-1}) and differences between experimental and calculated line positions in $10^{-3}cm^{-1}$, respectively. Columns 11 and 12 are the observed and calculated line intensities for a pure $CH_3{}^{35}Cl$ and $CH_3{}^{37}Cl$ isotopic species at 296 K in $cm^{-2}.atm^{-1}$. % is the difference (in percent) between experimental and calculated line intensities $[100\times(S_{obs}-S_{calc})/S_{obs}]$. An asterisk (*) corresponds to a transition overlapped with the previous one: the quoted calculated and measured intensities are for the total intensity of the overlapping lines.

Table 10:

Description of the generated linelist.

$CH_3{}^{35}Cl$

	V'	ℓ'	SILI	Total	Sig-Min	Sig-Max	Int-Min	Int-Max
	V1	**0**	2.390	2496	2920.03	3021.20	0.004	6.70
	V4	**1**	0.961	4461	2920.35	3197.76	0.004	2.00
	3V6	**1**	0.328	3469	2920.56	3192.75	0.004	1.60
	2V5	**2**	0.008	767	2920.07	3145.94	0.004	0.06
	3V6	**3**	0.004	114	2923.50	3084.75	0.004	0.33
	2V3+V5	**1**	0.003	19	2922.63	3002.75	0.004	1.10
Total			3.694	11326				

$CH_3{}^{37}Cl$

	V'	ℓ'	SILI	Total	Sig-Min	Sig-Max	Int-Min	Int-Max
	V1	**0**	0.760	2460	2920.03	3120.66	0.001	2.20
	V4	**1**	0.316	4359	2920.09	3196.35	0.001	0.64
	3V6	**1**	0.094	3318	2923.74	3197.96	0.001	0.48
	2V5	**2**	0.004	981	2920.03	3120.94	0.001	0.02
	3V6	**3**	0.002	322	2930.01	3159.10	0.001	0.13
	2V3+V5	**1**	0.002	197	2920.46	3010.79	0.001	0.24
Total			1.178	11637				

V' is the explicit mode notation of the bands use in HITRAN for CH_3Cl. SILI is the Sum of the Individual Line Intensities in 10^{-18} (cm^{-1}/(molecule.cm^{-2})) at 296 K. Total corresponds to the number of calculated lines. Sig-Min and Sig-Max: minimum and maximum values of the wavenumber (in cm^{-1}). Int-Min and Int-Max: minimum and maximum values of the intensity (in 10^{-21} (cm^{-1}/(molecule.cm^{-2})) at 296 K).

Table 11:
Comparison of the measured ν_1^0 line intensities between this work and Ref. [5].

Line	Isotope[a]	Wavenumber (cm^{-1})	S [b]	% [c]
		This work (measured)	This work (measured)	
$^{Q}P(2,42)$	241	2930.5831	0.483	-6.42
$^{Q}P(6,40)$	241	2930.6166	0.660	-9.70
$^{Q}P(9,34)$	241	2933.5933	0.526	-3.42
$^{Q}P(9,33)$	241	2934.4515	0.620	-2.26
$^{Q}P(2,37)$	241	2934.9384	0.112	-2.68
$^{Q}P(6,35)$	241	2934.9627	1.300	-2.15
$^{Q}P(9,31)$	241	2936.1697	0.750	-8.80
$^{Q}P(1,10)$	241	2958.8533	5.220	-7.85
$^{Q}P(1,10)$	242	2958.9689	1.640	-11.59
$^{Q}P(2,8)$	241	2960.4571	4.010	-10.47
$^{Q}P(2,8)$	242	2960.5453	1.290	-6.98
$^{Q}P(1,8)$	241	2960.6234	4.520	-7.52
$^{Q}P(1,8)$	242	2960.7117	1.400	-12.86
$^{Q}P(2,7)$	241	2961.3425	3.640	-9.62
$^{Q}P(2,7)$	242	2961.4170	1.120	-9.82
$^{Q}P(1,7)$	241	2961.5088	4.090	-9.05
$^{Q}P(3,6)$	241	2961.9511	4.580	-8.73
$^{Q}P(3,6)$	242	2962.0120	1.438	-8.07
$^{Q}P(2,5)$	241	2963.1140	2.470	-7.29
$^{Q}P(2,5)$	242	2963.1612	0.782	-9.46
$^{Q}P(3,4)$	241	2963.7229	18.640	-8.37
$^{Q}P(3,4)$	242	2963.7564	0.584	-14.73
$^{Q}P(2,4)$	241	2964.0000	1.790	-10.06
$^{Q}P(2,4)$	242	2964.0337	0.520	-20.58
$^{Q}P(1,4)$	241	2964.1664	2.380	-8.40
$^{Q}R(0,0)$	241	2968.6552	0.737	-2.04
$^{Q}R(2,2)$	241	2970.2071	9.650	-6.74
$^{Q}R(1,2)$	242	2970.3119	0.546	-13.55
$^{Q}R(0,2)$	241	2970.4293	2.090	-2.87
$^{Q}R(3,3)$	242	2970.7408	0.656	-3.35
$^{Q}R(3,3)$	241	2970.8167	2.040	-8.82
$^{Q}R(2,3)$	241	2971.0943	1.830	-12.02
$^{Q}R(1,3)$	242	2971.1855	0.764	-10.99
$^{Q}R(1,3)$	241	2971.2610	2.470	-10.53
$^{Q}R(9,22)$	241	2983.7734	1.184	-17.40
$^{Q}R(9,23)$	241	2984.6714	1.184	-7.09
$^{Q}R(9,28)$	241	2989.1645	0.930	-7.10

$^{Q}P(2,4)$: this notation stands for the transition $^{\Delta K}\Delta Q(K,J)$.

[a] : 241 and 242 corresponds to $CH_3{}^{35}Cl$ and $CH_3{}^{37}Cl$, respectively.

[b] : The values correspond to the measured lines intensities for natural CH_3Cl at 296K in 10^{-21} (cm^{-1}/(molecule.cm^{-2})).

[c] : % corresponds to $100\times (S_{\text{this work}}-S_{\text{Ref. [5]}})/S_{\text{this work}}$.

Table 12:

Comparison of the integrated intensities from PNNL and this work for various integration ranges.

	$S_{3\mu m}$(PNNL)	$^{Calc}S_{3\mu m}$	R=PNNL/This work
Integration range in cm^{-1}	PNNL [b]	This work	
2925-2976	0.204 [a]	0.208 [a]	0.980
2976-3027	0.187 [a]	0.188 [a]	0.976
3027-3078	0.075 [a]	0.076 [a]	0.989
3078-3129	0.040 [a]	0.039 [a]	1.016

[a] : in 10^{-17} cm^{-1}/(molecule.cm^{-2}) at 296 K.
[b]: Ref. [11].

Appendix: Definition of matrix elements of the effective rotation-vibration Hamiltonian.

- Diagonal in v operators: W(v;±ℓ) type operators
  - Terms diagonal in ℓ and K:

$$\left\langle \mathrm{v}\ell, J\,K \middle| H \middle| \mathrm{v}\ell, J\,K \right\rangle = E_{\mathrm{v}} + B_{\mathrm{v}}J(J+1) + (A_{\mathrm{v}} - B_{\mathrm{v}})K^2 - D_J^{\mathrm{v}}J^2(J+1)^2 - D_{JK}^{\mathrm{v}}JK^2(J+1) - D_K^{\mathrm{v}}K^4 + H_J^{\mathrm{v}}J^3(J+1)^3 + H_{JK}^{\mathrm{v}}J^2(J+1)^2K^2 + H_{KJ}^{\mathrm{v}}J(J+1)K^4 + H_K^{\mathrm{v}}K^6 + \left[-2A\zeta_{\mathrm{v}} + \eta_J^{\mathrm{v}}\,J\;\;J+1\;\; + \eta_k^{\mathrm{v}}K^2 + \ldots\right]K\ell \quad \text{(A1)}$$

The diagonal z-Coriolis terms $A\zeta_{\mathrm{v}}$ and its expansion ($\eta_{\mathrm{K}}^{\mathrm{v}}$ etc..) vanish for all ℓ=0 vibrational states.

  - Terms off-diagonal in ℓ:

For the ℓ =1 vibrational states the following (Δℓ ; Δ*K*)= (±2; ±2) and (Δℓ Δ*K*)= (±2; ∓1) -type operators were taken into account:

$$\left\langle \mathrm{v}\ell = \mp 1, J\;\; K \middle| q_{22} \middle| \mathrm{v}\ell' = \pm 1, J\,K' = K \pm 2 \right\rangle = M(v,\ell).\;\; q_{22}^1 + q_{22}^2\;\; K^2 + K'^2 \quad q_{22}.F_2^{\pm}(J,K) \quad \text{(A2)}$$

$$\left\langle \mathrm{v}\ell = \mp 1,\; J\,K \middle| c_{21,xz} \middle| \mathrm{v}\ell' = \pm 1, J\,K' = K \mp 1 \right\rangle = \;\; 2K \mp 1 \;\;\; c_{21,xz}^1 + c_{21,xz}^2 J(J+1) \;\; F_1^{\mp}(J,K) \quad \text{(A3)}$$

- Off diagonal in v operators
  - for (Δℓ ; Δ*K*)=(0; 0) operators

Anharmonic operators

$$\left\langle \mathrm{v}\ell,\; J\,K \middle| Anh \middle| \mathrm{v}'\ell' = \ell,\; J\,K' = K \right\rangle = \;\; Anh^0 + Anh^1K^2 + Anh^2J\;\; J+1\;\; + \ldots \quad \text{(A4)}$$

Z-type Coriolis resonance

$$\left\langle \mathrm{v}\ell, J\,K \middle| C_z \middle| \mathrm{v}\ell' = \ell, J\,K' = K \right\rangle = \;\; C_z^1 + C_z^2\,K^2 + \ldots \;\; \ell.K \quad \text{(A5)}$$

  - for (Δℓ ; Δ*K*)= (±1;±1) operators

$$\left\langle \mathrm{v}\ell,\; J\,K \middle| C_x \middle| \mathrm{v}'\ell' = \ell \pm 1, J\,K' = K \pm 1 \right\rangle = \left[\;\; C_x^1 + C_x^2 J(J+1) \;\pm\; 2K \pm 1 \;\;\; C_{yz}^1 + C_{yz}^2 \;\; K^2 + K'^2 \;\;\right] F_1^{\pm}(J,K) \quad \text{(A6)}$$

  - for (Δℓ ; Δ*K*)= (±1; ∓2) operators

$$\left\langle \mathrm{v}\,\ell,\ J\,K\left|C_{12}\right|\mathrm{v}'\,\ell'=\ell\pm1, J\,K'=K\mp2\right\rangle=\pm\left[\ C_{12}^{1}+C_{12}^{2}\ \ K^{2}+K'^{2}\ \ \right]F_{2}^{\mp}(J,K) \qquad \text{(A7)}$$

- for $(\Delta\ell\,;\,\Delta K)=(\pm2;\mp1)$ operators

$$\left\langle \mathrm{v}\,\ell,\ J\,K\left|C_{21}\right|\mathrm{v}'\,\ell'=\ell\pm2, J\,K'=K\mp1\right\rangle=\left[\pm\ C_{21,y}^{1}+C_{21,y}^{2}J\ \ J+1\ \ +\ 2K\pm1\ C_{21,xz}^{1}\right]F_{1}^{\pm}(J,K) \qquad \text{(A8)}$$

- for $(\Delta\ell\,;\,\Delta K)=(\pm2;\pm2)$ operators

$$\left\langle \mathrm{v}\,\ell, J\ K\left|Q_{22'}\right|\mathrm{v}'\,\ell'=\ell\pm2, J\,K'=K\pm2\right\rangle=\ Q_{22}^{0}+Q_{22}^{1}\ \ K^{2}+K'^{2}\ \ .F_{2}^{\pm}(J,K) \qquad \text{(A9)}$$

➢ Particular case for the $(\Delta\ell\,;\,\Delta K)=)=(\pm2;\pm2)$ off diagonal in ℓ operator for $(\mathrm{v}_6=3;\ell=\pm3\ )\Leftrightarrow(\mathrm{v}_6=3;\ell=\pm1)$.

$$\left\langle \mathrm{v}_6=3\,\ell=\pm1, J\ K\left|Q_{22}\right|\mathrm{v}'_6=3\ \ell'=\pm3, J\,K'=K\pm2\right\rangle= \quad Q_{22}^{\ell=3,\ell=1}+F_{22,K}^{\ell=3,\ell=1}\ \ K^{2}+K'^{2}\ \ .M(v,\ell).F_{2}^{\pm}(J,K) \qquad \text{(A10)}$$

$$F_{n}^{\pm}(J,K)=\prod_{i=1}^{n}\left[\ J\ \ J+1\ -\ K\pm i\mp1\ \ K\pm i\ \right]^{1/2}$$

$M\ \ v,\ell\ =\sqrt{\mathrm{v}-\ell\ \ \mathrm{v}+\ell+2}$, with $M(\mathrm{v}=1,\ell=-1)=2$, $M(\mathrm{v}=3,\ell=-1)=4$ and $M(\mathrm{v}=3,\ell=1)=2\sqrt{3}$

$$F_{n}^{\pm}(J,K)=\prod_{i=1}^{n}\left[\ J(J+1)-\ K\pm i\mp1\ \ K\pm i\ \right]^{1/2}$$

The phase convention is:

$$\left\langle J\,K\left|J_x\pm i\,J_y\right|J\,K\pm1\right\rangle=F_{1}^{\pm}(J,K)$$

Figure 1:

Overview of the ν_1^0, ν_4^1 and $3\nu_6^1$ band of methyl chloride in the 3.4 µm region. In the 2920-3150 cm^{-1} spectral region, the agreement of the present calculation (upper panel) with the observation (spectrum #3) is significantly improved as compared to the one obtained when using the linelist available in HITRAN [2] or GEISA [3] (lower panel). The present study does not concern the highly perturbed $2\nu_5^0$ band centered near 2880 cm^{-1}.

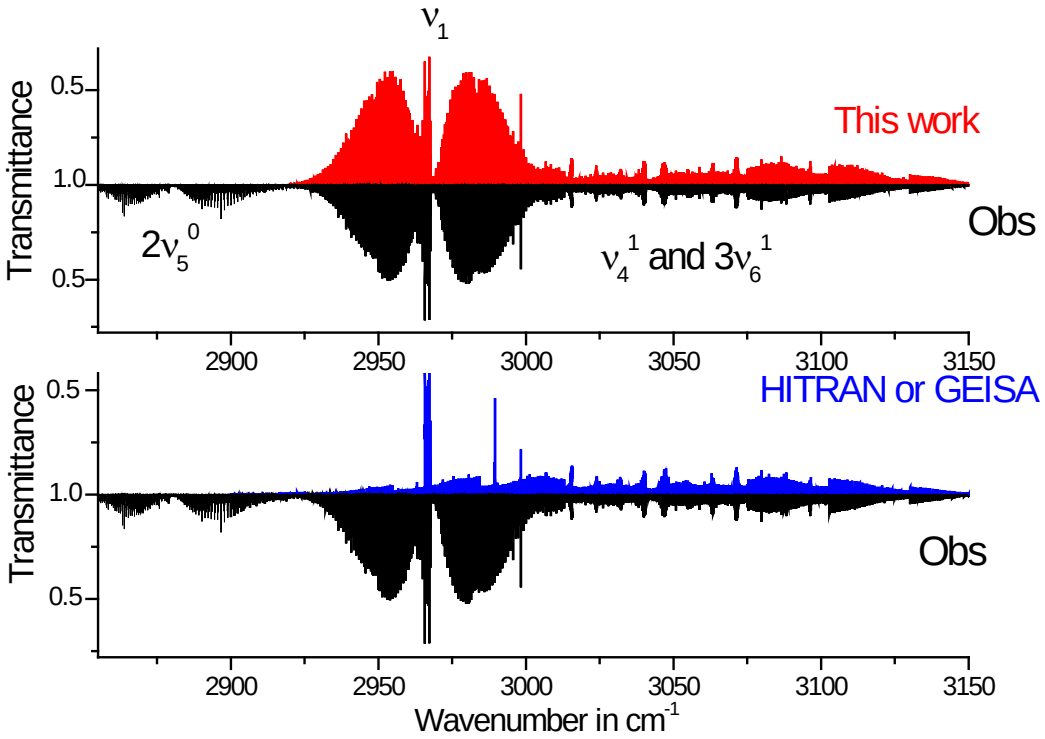

Figure 2:

Part of spectrum #3 near 2965 cm^{-1}. The strong $^{Q}Q_K$ (ΔJ = 0, ΔK=0) series of the $\nu_1{}^0$ band for K=1 to K=10 is indicated on the lower trace. All traces have the same vertical scale but are shifted for visual clarity.

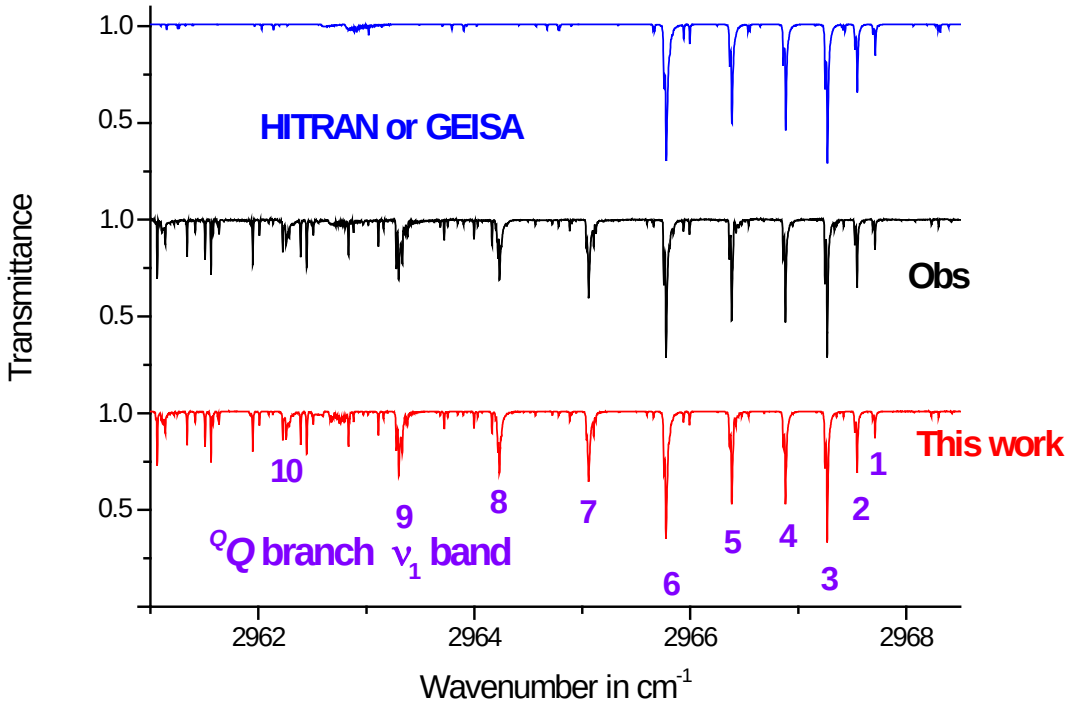

Figure 3:

Part of the ^{Q}P branch of the $\nu_1{}^0$ band in spectrum #3 near 2940 cm^{-1}. For K=0 the upper J' values are given and the transitions for $CH_3{}^{35}Cl$ and $CH_3{}^{37}Cl$ are marked by diamonds and triangles, respectively. All traces have the same vertical scale but are shifted for visual clarity.

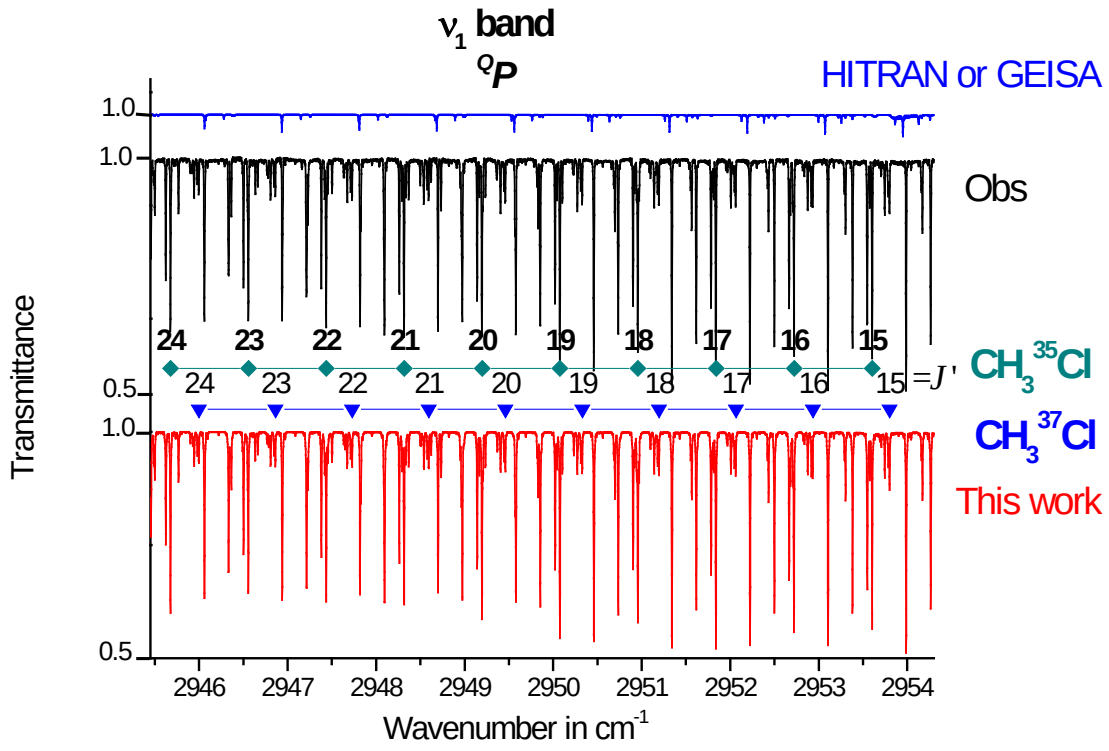

Figure 4:
Single channel spectra of CH_3Cl around 3000 cm^{-1}. The upper panel corresponds to spectrum #3 recorded without any optical filter (H_2O and CO_2 transitions are observed). The bottom panel corresponds to spectrum #4 recorded with an optical filter.

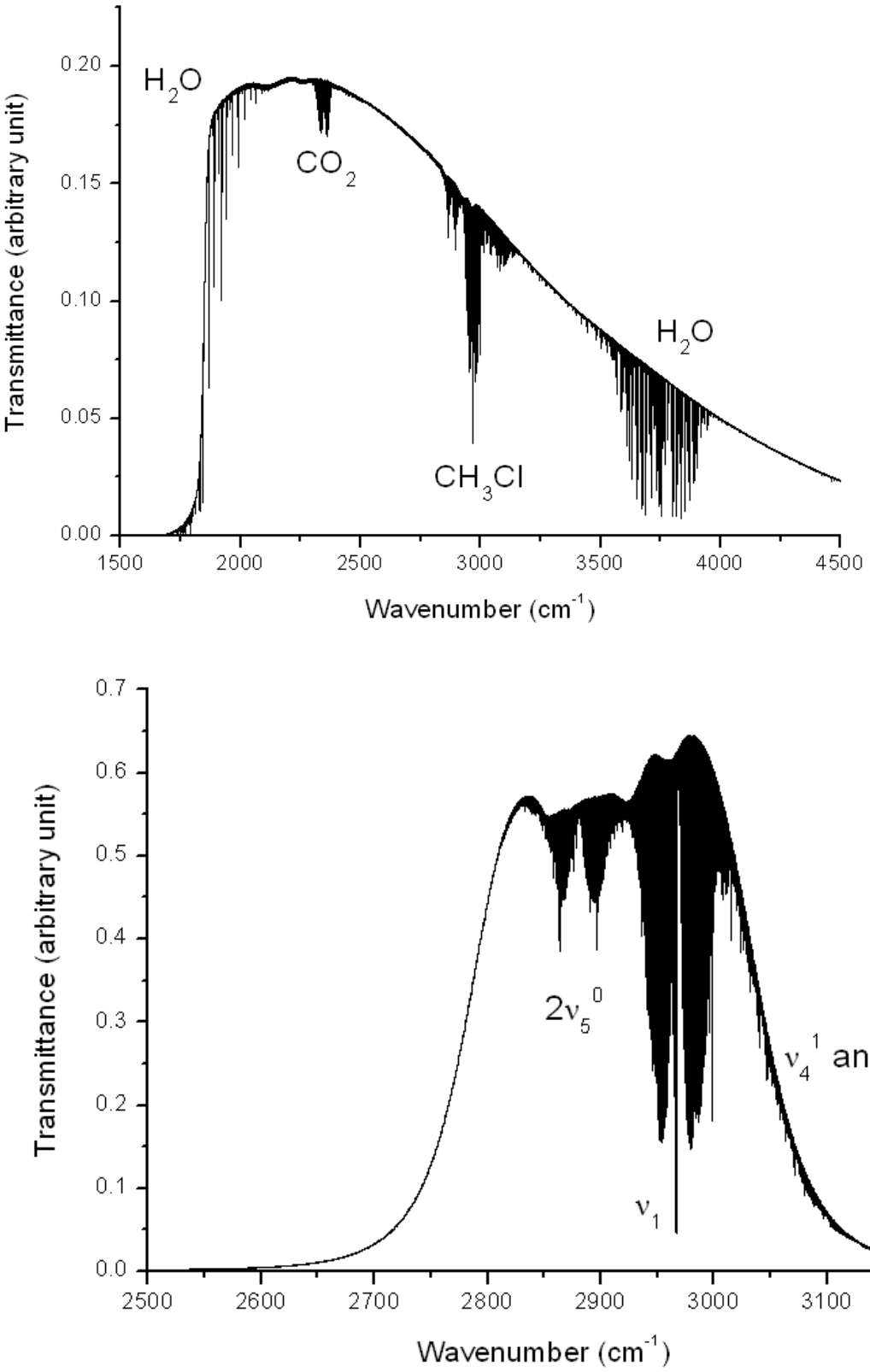

Figure 5:
Example of the simultaneous fit of two transitions from 6 experimental spectra (from lower to higher pressure, see Table 1) between 2931.18 and 2931.34 cm^{-1}.

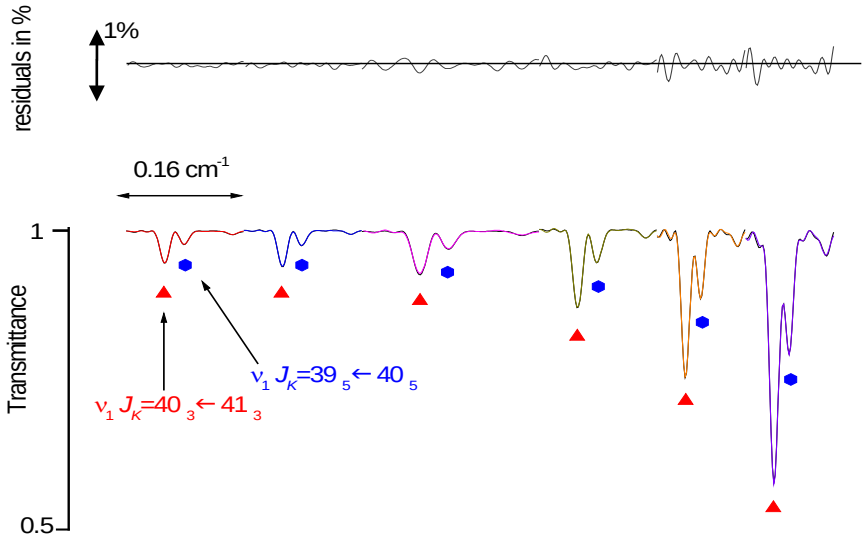

Figure 6:

Part of the methyl chloride spectrum near 2983 cm^{-1} (*R* branch of the $\nu_1{}^0$ band). The assignments are given for $CH_3{}^{35}Cl$ (circles) and $CH_3{}^{37}Cl$ (triangles). Because of a local resonance the forbidden $2\nu_3+\nu_5{}^1$ for $CH_3{}^{35}Cl$ [19 6 ← 19 5] (star) becomes observable. All traces have the same vertical scale but are shifted for visual clarity.

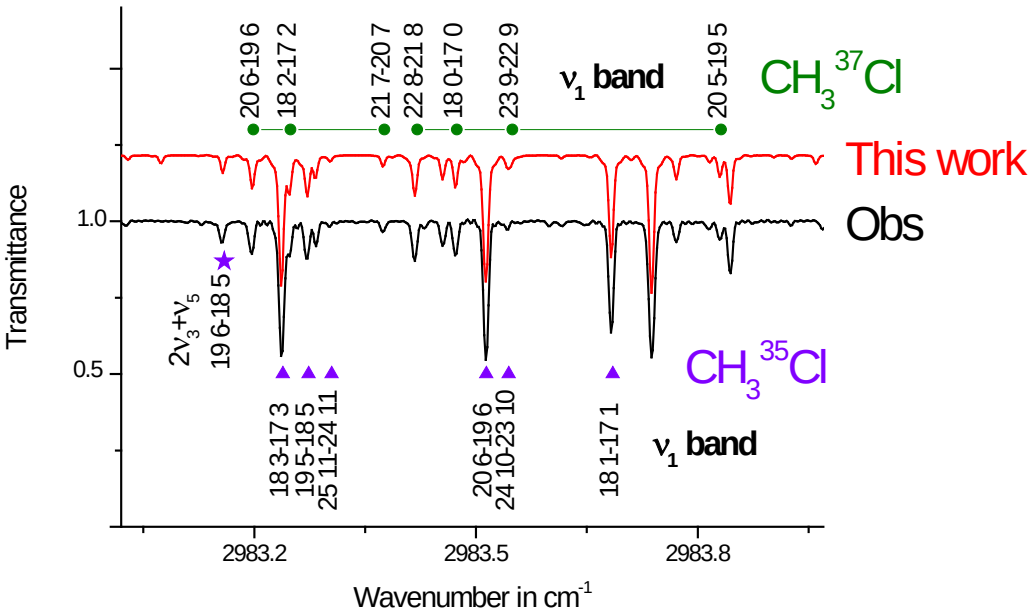

Figure 7:

Part of the methyl chloride spectrum near 3015 cm^{-1}: The lines of the ${}^{K'=2,\ell'=-1}Q_{K''=-3}(J)$ series of the $\nu_4{}^1$ band are clearly perturbed near J'~21. As a result, the $3\nu_6{}^3$ [21 0← 21 3] transition is clearly observable. For both series of assigned lines, the upper state J' values are indicated. All traces have the same vertical scale but are shifted for visual clarity.

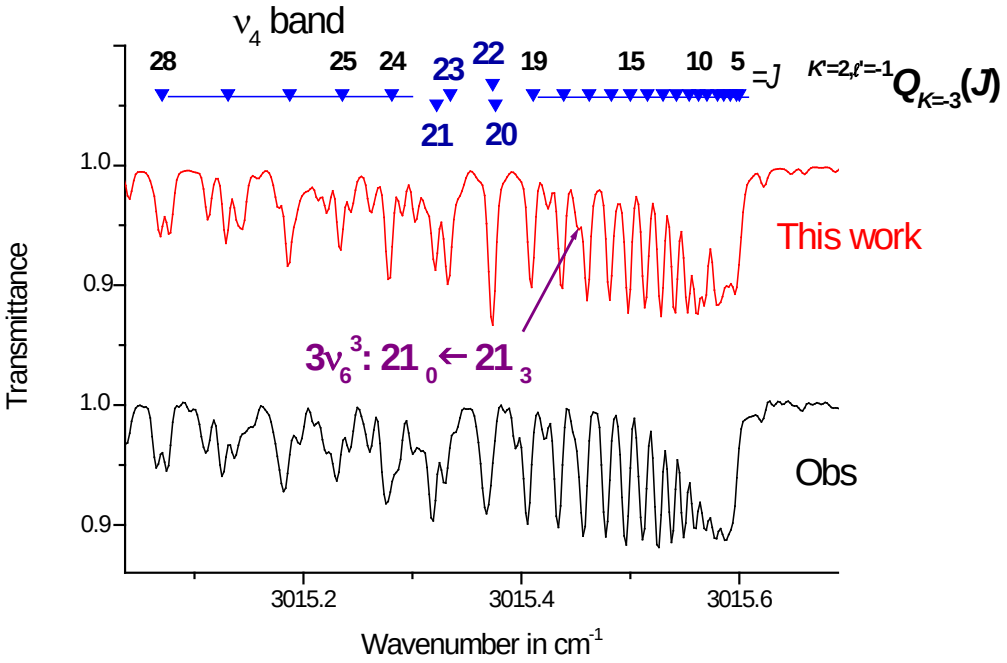

Figure 8:

Part of the methyl chloride spectrum near 3150 cm^{-1} ($^{R}Q_K$ branch of the $\nu_4{}^1$ band). Lines from the $3\nu_6{}^1$ band are also observable. All traces have the same vertical scale but are shifted for visual clarity.

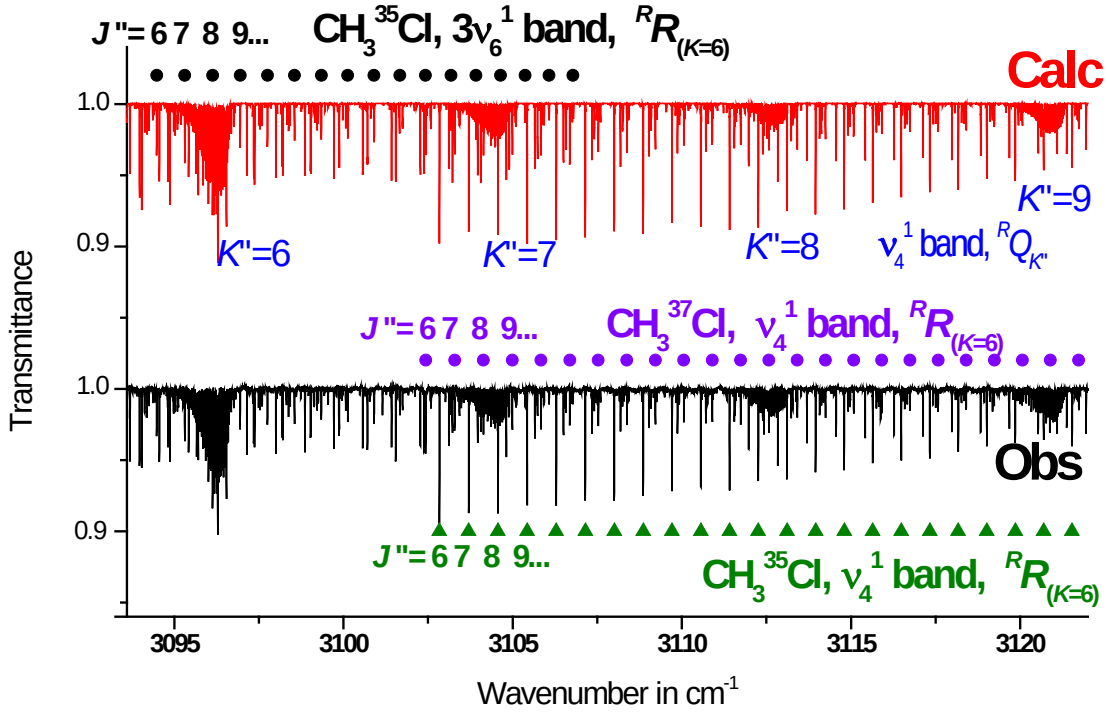

Figure 9:
Analysis of the resonances perturbing the (v_4=1; ℓ =±1) energy levels for J =21 and Γ=A_1 or A_2 symmetry. The mixing coefficient % (A_1, (v_4=1; ℓ =±1), J '=21 K '| v ℓ), in percentage (see text) on the (v_6=3; ℓ =±1), (v_6=3; ℓ =±3) and (v_0=1; ℓ =0) interacting vibrational states. There exists a local resonance coupling together (v_4=1; ℓ =±1), K=-2 ⇔ (v_6=3; ℓ =±3) K=0.